SUPPLEMENTARY INFORMATION

Advanced Framework-Modified POM@ZIF-67 Nanocomposites as Enhanced Oxygen Evolution Reaction (OER) Electrocatalysts.

Víctor K. Abdelkader-Fernández,* Diana M. Fernandes,*

Salete S. Balula, Luís Cunha-Silva* and Cristina Freire

REQUIMTE/LAQV, Departamento de Química e Bioquímica, Faculdade de Ciências da Universidade de Porto, Rua do Campo Alegre, 4169-007 Porto, Portugal.

1. EXPERIMENTAL DETAILS

1.1. POM@ZIF nanocomposites – Materials and methods

Reagents and solvents. Cobalt nitrate hexahydrate ($Co(NO_3)_2 \cdot 6H_2O$, ACS reagent, ≥98%, Sigma-Aldrich) and 2-methylimidazole – 2-MeIm – ($C_4H_6N_2$, 99%, Sigma-Aldrich) were employed as received as ZIF-67 precursors. Ruthenium (IV) oxide (RuO_2, 99.9%, Sigma-Aldrich) and iridium (IV) oxide (IrO_2, 99.9%, Sigma-Aldrich) were used as OER benchmark references. Methanol (CH_3OH, analytical reagent grade, ≥99.9%, Fisher Scientific) and ultrapure water were used as solvents.

POM preparations.

The two cobalt tri-substituted analogue salts (with potassium and TBA as counterions)—$K_3Na_3H_4[SiW_9Co_3(H_2O)_3O_{37}] \cdot 13H_2O$ and $(TBA)_6H_4[SiW_9Co_3(H_2O)_3O_{37}] \cdot H_2O$, abbreviated as SiW_9Co_3 and TBA-SiW_9Co_3, respectively—were prepared following the procedure already described in our previously published work.[1] Also, the preparation of potassium and TBA salts of mono-substituted silicotungstate ($K_4H_2[SiW_{11}Co(H_2O)O_{39}] \cdot 22H_2O$ and $TBA_4H_2[SiW_{11}Co(H_2O)O_{39}] \cdot H_2O$, abbreviated as $SiW_{11}Co$ and TBA-$SiW_{11}Co$, respectively) was performed following procedures previously reported.[2]

Characterization techniques. Inductively coupled plasma - optical emission spectrometry (ICP-OES) analysis were registered with a spectrometer Optima 4300 DV (Perkin Elmer) with plasma source (RF generator of 40 Hz), and automatic sampler (PerkinElmer AS93-plus). ICP-OES analysis were performed at "*Centro de Apoyo Científico-Tecnológico (CACTUS) de la Universidad de Santiago de Compostela, USC (Galicia, Spain)*".

X-ray photoelectron spectroscopy (XPS) spectra were recorded at "*Centro de Materiais da Universidade do Porto, CEMUP (Porto, Portugal)"*, on a Kratos Axis Ultra HAS spectrometer using monochromatic AlKα radiation (1486.6 eV). XPS data treatment was performed by using the CasaXPS software (version 2.3.16, Casa Software Ltd.). The C1s transition at 284.6 eV was used as internal reference. Surface atomic concentrations for the different elements were obtained from the corresponding peak areas (in XPS high resolution spectra) and using the relative sensitivity factors (RSF) provided by the manufacturer. The high resolution XPS spectra were deconvoluted via Levenberg–Marquardt algorithm, i.e., non-linear least squares curve fitting.

Fourier Transform infrared (FT-IR) spectra were recorded on a Jasco FT/IR-460 Plus spectrophotometer in the range 400 - 4000 cm^{-1}, using a resolution of 4 cm^{-1} and 64 scans.

Powder X-ray diffraction (PXRD) analyses were performed at "*Instituto de Física dos Materiais da Universidade do Porto, IFIMUP (Porto, Portugal)*". PXRD patterns were obtained with a Rigaku Smartlab

X-ray Diffractometer, involving a X-ray source CuKα (λ = 1.5418 Å; acceleration potential = 45 kV; current = 200 mA). A Bragg-Brentano geometry was used.

Nitrogen-adsorption/desorption isotherms were recorded by using a Micromeritics' Gemini VII 2390 surface area analyser at CICECO (University of Aveiro, Aveiro, Portugal). The analyses were performed at 77 K and, previously, the samples were degassed for 6 hours, under vacuum at 150 °C.

Scanning electronic microscopy (SEM) micrographs and energy-dispersive X-ray (EDS) spectra and mappings for the different elements were collected at CEMUP (Porto, Portugal), using a high resolution (Schottky) environmental microscope with X-ray microanalysis and backscattered electron diffraction pattern analysis (FEI Quanta 400FEG/EDAX Genesis X4 M). Measures were carried out under high-vacuum conditions.

Transmission electronic microscopy (TEM) images were captured with a high resolution TEM (Hitachi, H9000 NAR), equipped with thermionic emission electron cannon and CCD camera, at Centro de Investigação em Materiais Cerâmicos e Compósitos – CICECO – University of Aveiro (Aveiro, Portugal). TEM/EDS element distribution maps were acquired also at CICECO by using a JEM-2200FS Field Emission Electron Microscope (JEOL) equipped with a 200kV field emission gun (FEG) and in-column energy filter (Omega filter).

1.2. Assessment of electrochemically active surface areas (ECSA)

ECSA values exhibited by electrocatalysts are usually calculated by using the equation:

$$ECSA = C_{dl} / C_{ref}$$

where C_{dl} stands for the double-layer capacitance and C_{ref} for the reference capacitance value per unit area. Usually, due to the impossibility of knowing the exact C_{ref} value for specific and structurally complex materials, the majority of reported studies based their *ECSA* evaluations on a straight comparison of the corresponding C_{dl} values, assuming that C_{ref} for all the studied materials are similar, i.e., ranging in the same order of magnitude. However, the different structures and compositions of the samples considered in this work (pristine ZIF-67, nanocomposite materials—presenting low and high POM loadings—and the commercial benchmark references) does not allow assume their corresponding reference capacitances are comparable. This fact makes mandatory the calculation of these C_{ref} values, although they will necessarily be mere approximations, in order to perform a more reliable comparison of the electrochemically active surface areas.

Calculation of double-layer capacitances (C_{dl})

C_{dl} values were calculated via standard double-layer charging test, namely, acquisition of consecutive CV plots at different scan rates (from 20 to 160 $mV \cdot s^{-1}$), being the double-layer capacitance estimated

from the slope of linear-fitted plot of current density at 0.8 V *vs.* RHE - $j_{0.8}$ - (non-faradaic region) versus the scan rate (*k*):

$$j_{0.8} = C_{dl} \cdot k$$

Calculation of 'estimative' reference capacitances (C_{ref})

Firstly, specific capacitance values for all the materials were calculated from the corresponding CV data and by using the formula:

$$C = Q / (2 \cdot V \cdot m)$$

where *C* stands for specific capacitance (expressed in F g^{-1}), *Q* for the charge (in A s), *V* for the potential range (in V), and *m* for the mass of sample deposited on the electrode surface (in g). At the same time Q values were obtained by the equation:

$$Q = A / k$$

where *A* corresponds to the area under the curve of the CV plot (expressed in A V), and *k* to the scan rate (in V s^{-1}). Then, these calculated *C* values were referred to the specific area of the material to find their corresponding reference capacitances, C_{ref}, expressed in F m^{-2}. For these calculations, BET surface areas (m^2 g^{-1}) were obtained from the corresponding N_2-adsorption isotherms of ZIF-67 and POM@ZIF-67 nanocomposites, as well as the typical—previously reported—values for the benchmark materials: RuO_2 (≈11 m^2/g) and IrO_2 (≈5 m^2/g).[3]

In all these calculations several error sources contribute to the global uncertainty of the reference capacitances and, consequently, to the finally calculated *ECSA* values. For instance, even if no redox peaks appeared into the CV plots faradaic contributions could not be completely negligible, increasing the measured CV areas and subsequently, leading to overestimated charges and capacitance values. Since the magnitude of faradaic contributions is influenced by a plethora of experimental factors (electrolyte composition, temperature, pH, scan rate, etc.), slight variations in some of these conditions can result in significant changes in the calculated C_{ref} values. Moreover, the use of BET surface values (depending on the N_2 molecules accessibility) in the calculations of electrochemically active surface areas (depending on the accessibility of the electrolyte) entails the assumption that these two types of area values are comparable. Taking in account these considerations, the *ECSA* values calculated in this work are estimative, but regarding the scope of the study provides the enough accuracy to be used for comparative purposes.

2. OCCUPANCY CALCULATION

The calculation of the occupancy degrees for each 'in situ'-prepared POM@ZIF-67 nanocomposite—expressed as POM units per 100 ZIF cages—is based on:

i. amounts of POM units detected into the nanocomposites (POM unit per gram of nanocomposite) calculated from W contents measured by ICP-OES analysis;

ii. mass of ZIF-67 in each nanocomposite calculated by subtracting the mass of POM to the total nanocomposite mass;

iii. each ZIF-67 cage (unit cell) is formed by 24 Co nodes. However, since all the cobalt nodes are shared by two adjacent cages, the effective number of Co nodes per ZIF-67 cage is 12. Thereupon, the number of ZIF-67 cages per gram of nanocomposite can be calculated from the mass of ZIF-67 in the nanocomposite by using their molar mass—$Co(C_8H_{10}N_4)$, 221.12 g mol^{-1}—the stoichiometric relation of Co nodes per mole of ZIF-67 (1:1) and the known value of 12 metal nodes per unit cell;

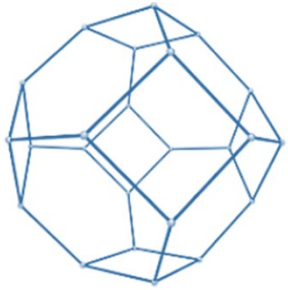

Schematic representation of ZIF-67-unit cell structure (truncated octahedron), where metallic node positions / vertices are marked with red dots.

iv. Finally, when the amount of POM units and ZIF-67-cages present in the POM@ZIF-67 sample have been found, the Occupancy degree can be calculated directly:

$$\textit{Occupancy (\%)} = [(\textit{POM units/g nanocomposite}) / (\textit{ZIF-cages/g nanocomposite})] \times 100$$

3. TABLES

Table S1. Proposed assignations of chemical moieties for the components obtained by XPS high resolution spectra curve fitting. Components are labelled as in Table S2 and Figure S3.

Element	Component	Assignation	
K 1s	K**1**	**K(I)**	*from POM salt*
C 1s	C**1**	**C–C**	*from adventitious carbon* [4]
		C–C	*from 2–methylimidazole – ZIF-67* [5, 6]
		C–N	*from 2-methylimidazole – ZIF-67* [5]
	C**2**	**C**–O	*from adventitious carbon* [4]
	C**3**	O–**C**=O	*from adventitious carbon* [4]
		CO_3^{2-}	*from ZIF-67* [6]
	C**4**	**C**–$(N)_2$	*from 2-methylimidazole – ZIF-67* [5, 7]
		C–O	*from adventitious carbon* [4]
O 1s	O**1**	**O**–W	*from POM cluster*
	O**2**	**O**–Co	*from POM cluster*
		O–Si	*from POM cluster*
	O**3**	C–**O**	*from adventitious carbon* [4]
	O**4**	N**O**$_3^-$	*from ZIF-67* [8]
	O**5**	–**O**H	*from ZIF-67* [6]
		H_2**O**–(Co)	
N 1s	N**1**	**N**–$(C)_2$	*from 2-methylimidazole – ZIF-67* [5-7]
	N**2**	**N**–H / **N**H_4^+	*from ZIF-67* [6, 9]
	N**3**	**N**O_3^-	*from ZIF-67* [10]
Co 2p	Co**1**	**Co(II)**	*from ZIF-67* [11]
		Co–O	*from POM cluster*
	Co**2**	Satellite	
Si 2s	Si**1**	**Si**–O	*from POM cluster*
W 4f	W**1**	**W**–O	*from POM cluster* [12]
	W**2**	Loss feature	

Table S2. Core-level binding energies (BE) for all the 'pure' and nanocomposite samples obtained by curve fitting of XPS spectra. Components are labelled as in Table S1 and Figure S3.

Sample	Element	BE (eV)*				
$SiW_{11}Co$	K 2p	K**1** [3/2] 293.0(1.314)	K**1** [1/2] 295.8(1.314)			
	C 1s	C**1** 284.8(1.406)	C**2** 286.2(1.406)	C**3** 288.7(1.406)		
	O 1s	O**1** 530.6(1.300)	O**2** 532.5(1.300)			
	Co 2p	Co**1** [3/2] 781.0(2.567)	Co**1** [1/2] 796.7(2.567)	Co**2** [3/2] 784.9(8.658)	Co**2** [1/2] 804.0(8.658)	
	Si 2s	Si1 153.0(1.390)				
	W 4f	W**1** [7/2] 35.7(0.984)	W**1** [5/2] 37.9(0.984)	W**2** 41.3(2.239)		
SiW_9Co_3	K 2p	K**1** [3/2] 293.0(1.393)	K**1** [1/2] 295.8(1.393)			
	C 1s	C**1** 284.7(1.388)	C**2** 286.2(1.388)	C**3** 288.4(1.388)		
	O 1s	O**1** 530.5(1.497)	O**2** 532.3(1.497)			
	Co 2p	Co**1** [3/2] 781.3(2.786)	Co**1** [1/2] 797.0(2.786)	Co**2** [3/2] 786.0(5.536)	Co**2** [1/2] 802.5(5.536)	
	Si 2s	Si**1** 153.0(1.470)				
	W 4f	W**1** [7/2] 35.7(1.193)	W**1** [5/2] 37.8(1.193)	W**2** 41.2(3.334)		
ZIF-67	C 1s	C**1** 284.9(1.362)		C**3** 288.4(1.362)	C**4** 286.1(1.362)	
	O 1s			O**3** 531.6(1.715)	O**4** 532.6(1.715)	O**5** 534.1(1.715)
	N 1s	N**1** 399.1(1.268)	N**2** 400.7(1.268)	N**3** 406.9(1.268)		
	Co 2p	Co**1** [3/2] 781.4(2.472)	Co**1** [1/2] 797.1(2.472)	Co**2** [3/2] 786.4(5.696)	Co**2** [1/2] 802.1(5.696)	

$SiW_{11}Co$@ZIF-67	C 1s	C**1**		C**3**	C**4**	
		284.7(1.140)		288.5(1.140)	285.9(1.140)	
	O 1s	O**1**	O**2**	O**3**	O**4**	O**5**
		530.5(1.500)	532.3(1.500)	531.5(1.500)	533.3(1.500)	534.1(1.500)
	N 1s	N**1**	N**2**	N**3**		
		398.9(1.265)	400.5(1.265)	407.5(1.265)		
	Co 2p	Co**1** [3/2]	Co**1** [1/2]	Co**2** [3/2]	Co**2** [1/2]	
		781.1(2.484)	796.8(2.484)	785.9(6.129)	801.6(6.129)	
	Si 2s	Si**1**				
		152.8(1.300)				
	W 4f	W**1** [7/2]	W**1** [5/2]	W**2**		
		35.3(1.112)	37.5(1.112)	40.8(2.917)		
$SiW_{11}Co[h]$@ZIF-67	C 1s	C**1**		C**3**	C**4**	
		284.8(1.383)		288.3(1.383)	286.1(1.383)	
	O 1s	O**1**	O**2**	O**3**	O**4**	O**5**
		530.3(1.768)	532.3(1.768)	531.5(1.768)	532.7(1.768)	533.7(1.768)
	N 1s	N**1**	N**2**	N**3**		
		399.1(1.375)	400.5(1.375)	406.8(1.375)		
	Co 2p	Co**1** [3/2]	Co**1** [1/2]	Co**2** [3/2]	Co**2** [1/2]	
		781.3(2.538)	797.0(2.538)	786.3(6.782)	802.0(6.782)	
	Si 2s	Si**1**				
		153.2(1.300)				
	W 4f	W**1** [7/2]	W**1** [5/2]	W**2**		
		35.3(1.125)	37.5(1.125)	41.2(3.249)		
SiW_9Co_3@ZIF-67	C 1s	C**1**		C**3**	C**4**	
		284.8(1.210)		288.3(1.210)	285.9(1.210)	
	O 1s	O**1**	O**2**	O**3**	O**4**	O**5**
		530.7(1.456)	532.3(1.456)	531.5(1.456)	532.8(1.456)	534.1(1.456)
	N 1s	N**1**	N**2**	N**3**		
		399.0(1.249)	400.6(1.249)	407.3(1.249)		
	Co 2p	Co**1** [3/2]	Co**1** [1/2]	Co**2** [3/2]	Co**2** [1/2]	
		781.3(2.595)	797.0(2.595)	786.2(5.978)	801.9(5.978)	
	Si 2s	Si**1**				
		153.1(1.310)				
	W 4f	W**1** [7/2]	W**1** [5/2]	W**2**		
		35.4(1.207)	37.6(1.207)	40.6(5.000)		

SiW_9Co_3[h]@ZIF-67	C 1s	C**1**		C**3**	C**4**	
		284.8(1.458)		288.3(1.458)	285.9(1.458)	
	O 1s	O**1**	O**2**	O**3**	O**4**	O**5**
		530.3(1.624)	532.4(1.624)	531.5(1.624)	532.7(1.624)	534.1(1.624)
	N 1s	N**1**	N**2**	N**3**		
		398.9(1.327)	400.5(1.327)	406.7(1.327)		
	Co 2p	Co**1** [3/2]	Co**1** [1/2]	Co**2** [3/2]	Co**2** [1/2]	
		781.2(2.604)	796.9(2.604)	786.2(6.434)	801.9(6.434)	
	Si 2s	Si**1**				
		152.8(1.200)				
	W 4f	W**1** [7/2]	W**1** [5/2]	W**2**		
		35.1(1.183)	37.3(1.183)	40.6(3.261)		

* The values between brackets refer to the full width at half-maximum (FWHM) of the bands.

Table S3. Surface-related parameters obtained from nitrogen adsorption isotherm data for ZIF-67 and POM@ZIF-67 nanocomposites.

Sample	Textural parameter		
	BET[a] *surface area* ($m^2\ g^{-1}$)	*BJH*[b] *pore volume*[c] ($cm^3\ g^{-1}$)	*BJH*[b] *pore width*[c] (nm)
ZIF-67	1490.5	0.445	1.96
$SiW_{11}Co$@ZIF-67	662.7	0.290	3.28
$SiW_{11}Co$[h]@ZIF-67	202.1	0.172	4.91
SiW_9Co_3@ZIF-67	957.6	0.356	2.60
SiW_9Co_3[h]@ZIF-67	62.8	0.133	8.93

[a]Brunauer-Emmett-Teller. [b]Barrett-Joyner-Halenda. [c]Calculated from adsorption data.

Table S4. Capacitance and area values of the commercial reference materials.

Sample	Area-related parameter			
	C_{ref} (µF cm^{-2}) [a]	C_{dl} (µF)[b]	*ECSA* (m^2 g^{-1})[c]	*Rf*[d]
ZIF-67	0.017	2.35	494	1957
$SiW_{11}Co$@ZIF-67	0.043	1.97	163	647
$SiW_{11}Co$[h]@ZIF-67	0.321	4.93	55	217
SiW_9Co_3@ZIF-67	0.019	1.62	308	1221
SiW_9Co_3[h]@ZIF-67	0.881	3.62	15	58
RuO_2	20.222	44.70	8	31
IrO_2	7.805	9.60	5	17

[a]Reference capacitances per unit area. [b]Double-layer capacitance values. [c]Electrochemically active surface areas. [d]Roughness factors. For details and calculations see Experimental Section of SI.

4. FIGURES

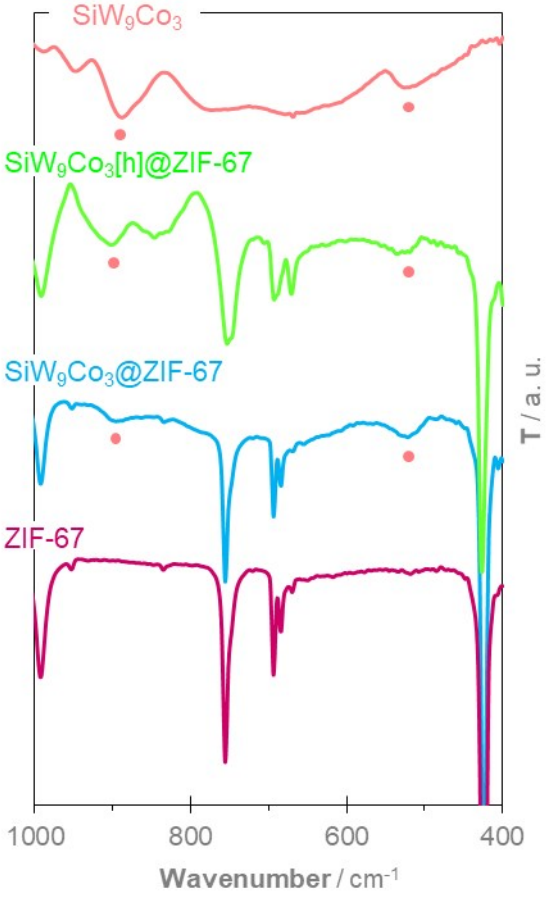

Figure S1. ATR-FTIR spectra of SiW_9Co_3, ZIF-67 and their two related nanocomposites—pink circle marks point to the characteristic vibrational bands of POM.

C 1s – K 2p

core-level regions

ZIF-67

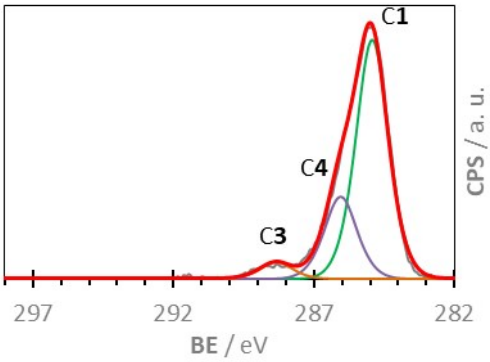

$SiW_{11}Co$

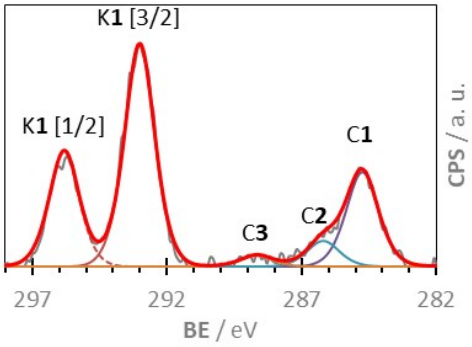

SiW_9Co_3

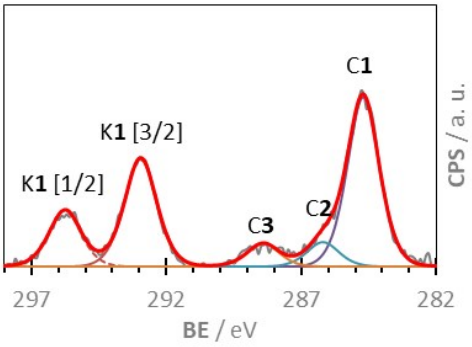

$SiW_{11}Co$@ZIF-67

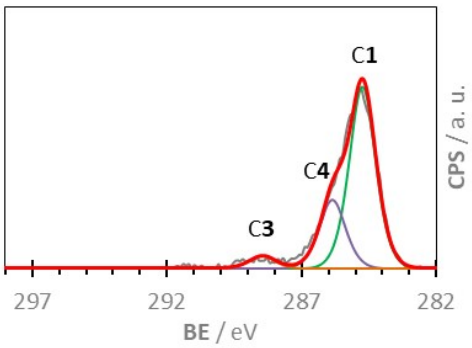

SiW_9Co_3@ZIF-67

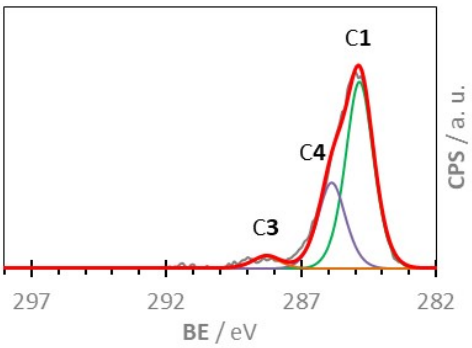

$SiW_{11}Co[h]$@ZIF-67

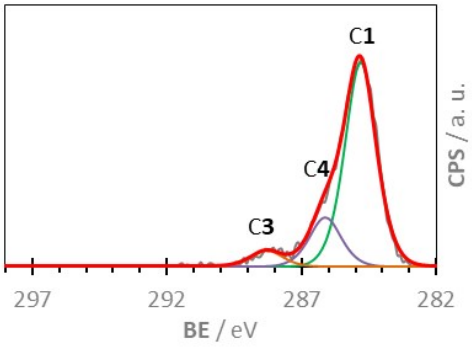

$SiW_9Co_3[h]$@ZIF-67

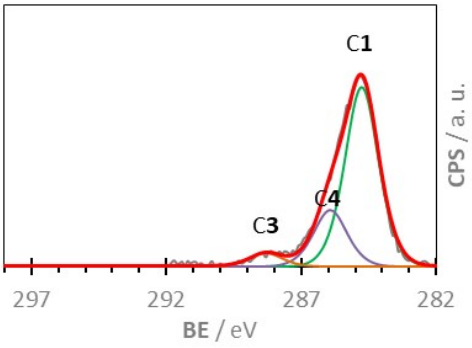

O 1s

core-level regions

ZIF-67

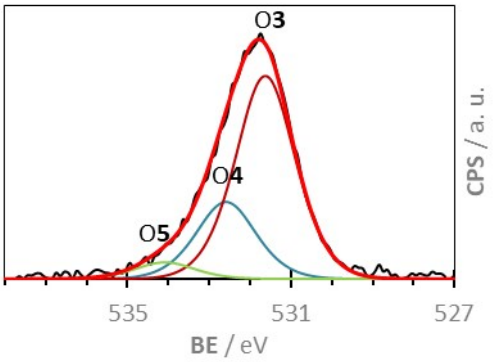

$SiW_{11}Co$

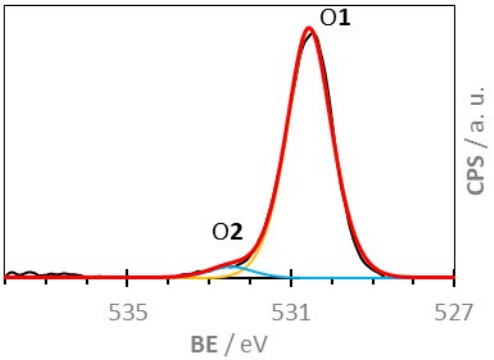

SiW_9Co_3

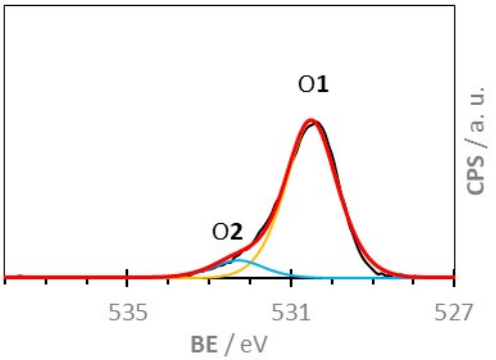

$SiW_{11}Co$@ZIF-67

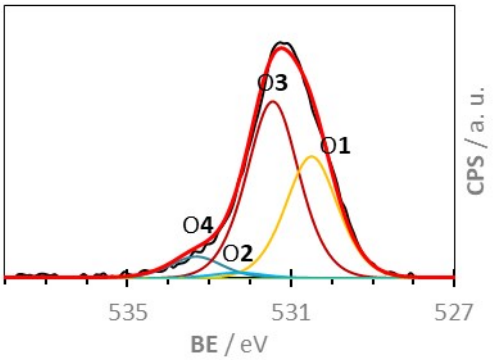

SiW_9Co_3@ZIF-67

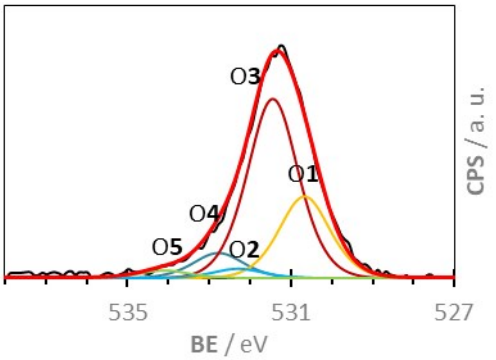

$SiW_{11}Co$[h]@ZIF-67

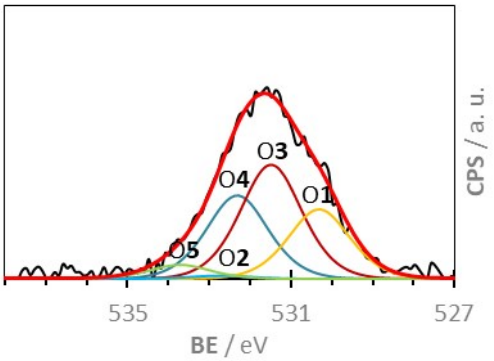

SiW_9Co_3[h]@ZIF-67

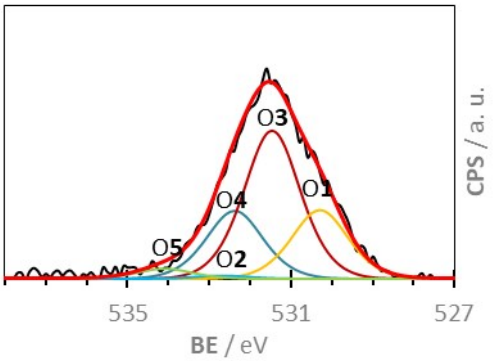

Co 2p

core-level regions

ZIF-67

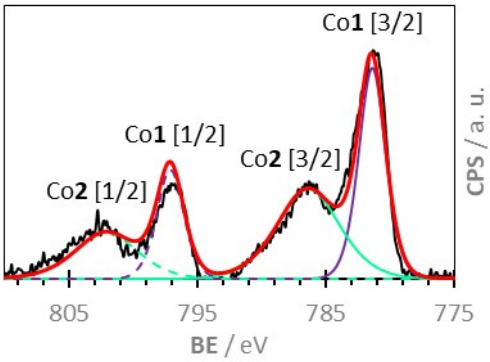

$SiW_{11}Co$

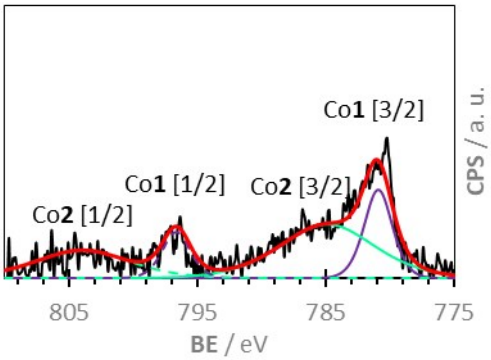

SiW_9Co_3

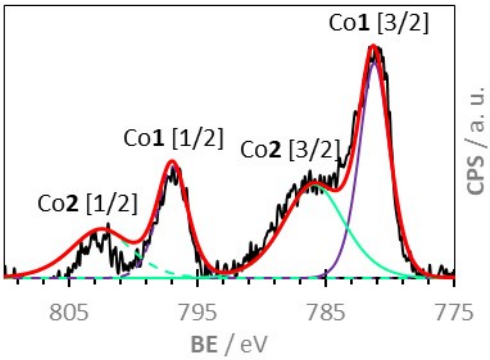

$SiW_{11}Co$@ZIF-67

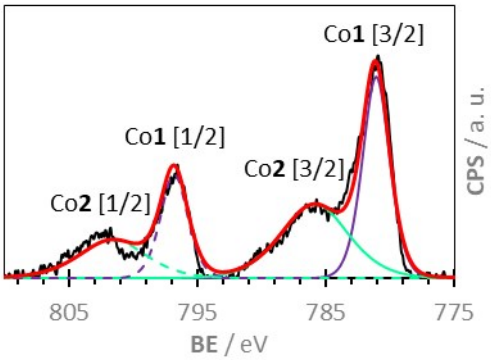

SiW_9Co_3@ZIF-67

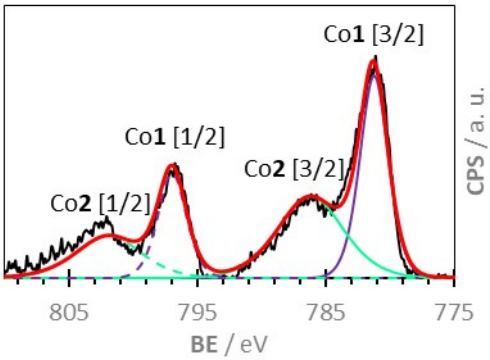

$SiW_{11}Co[h]$@ZIF-67

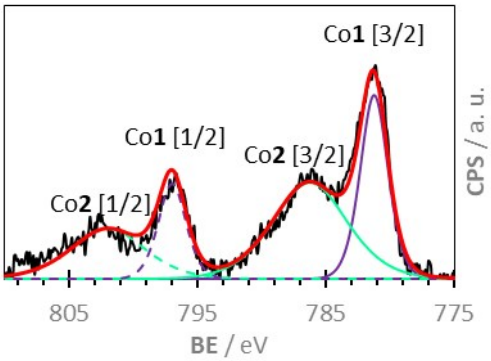

$SiW_9Co_3[h]$@ZIF-67

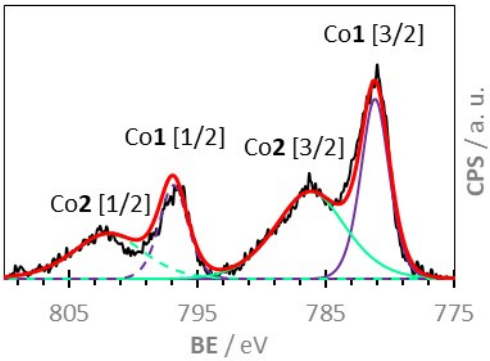

Si 2s

core-level regions

ZIF-67

$SiW_{11}Co$

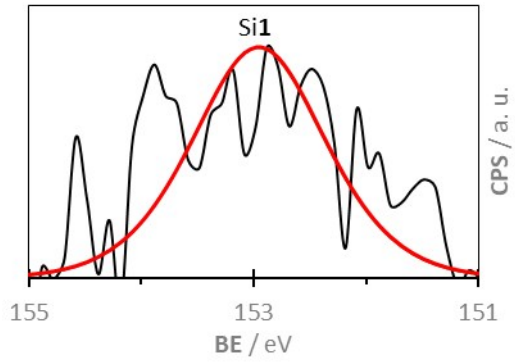

SiW_9Co_3

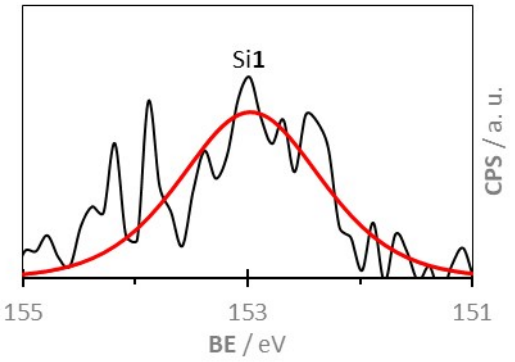

$SiW_{11}Co$@ZIF-67

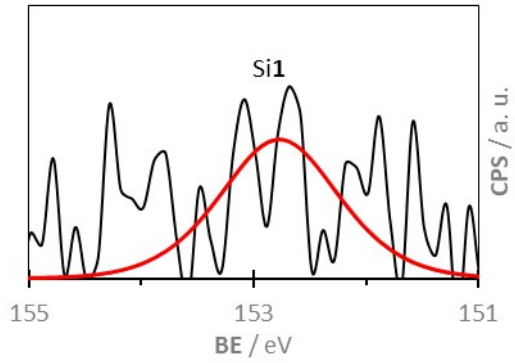

SiW_9Co_3@ZIF-67

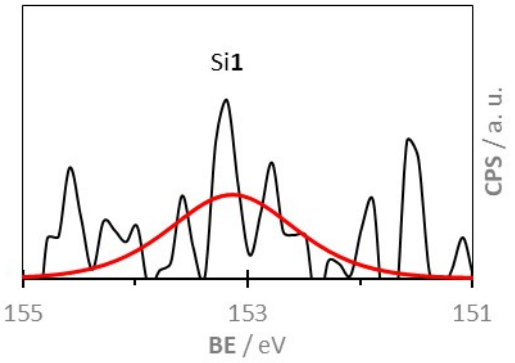

$SiW_{11}Co$[h]@ZIF-67

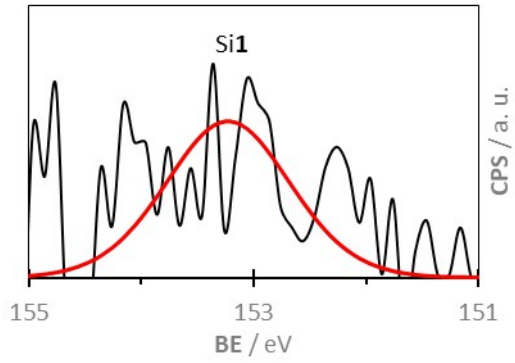

SiW_9Co_3[h]@ZIF-67

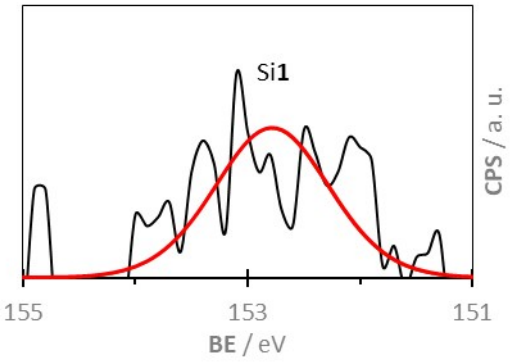

W 4f

core-level regions

ZIF-67

$SiW_{11}Co$

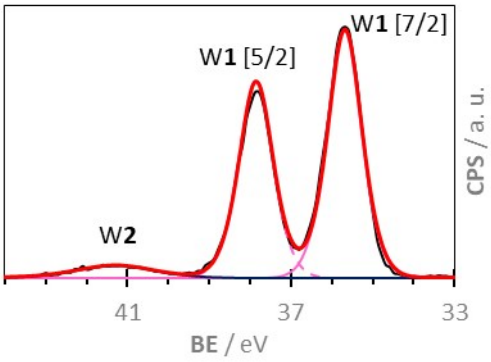

SiW_9Co_3

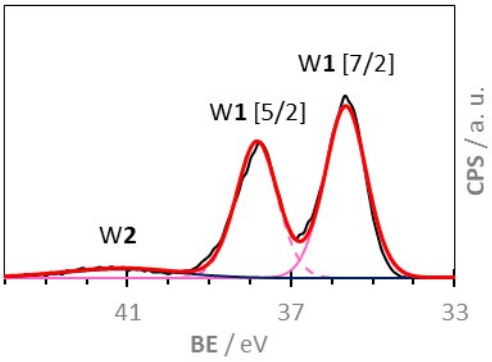

$SiW_{11}Co$@ZIF-67

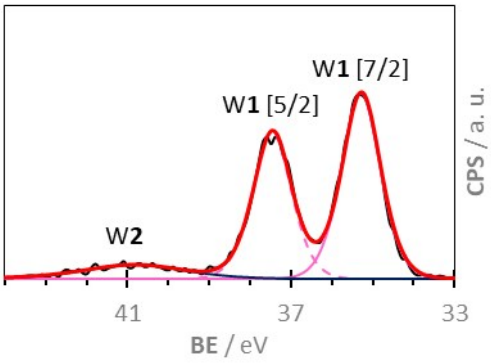

SiW_9Co_3@ZIF-67

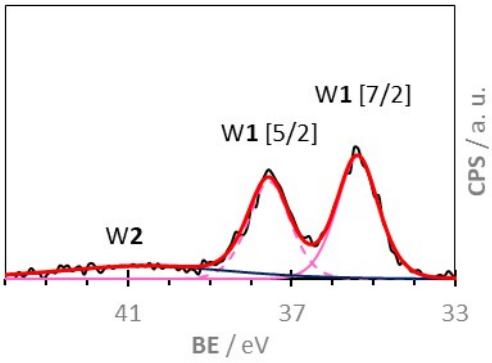

$SiW_{11}Co[h]$@ZIF-67

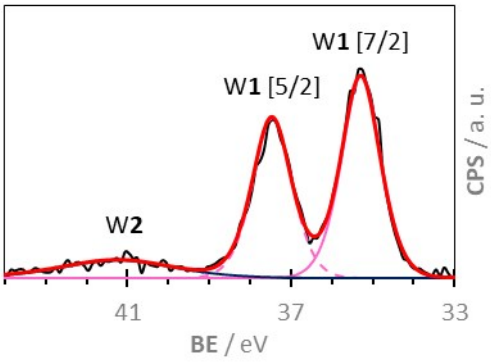

$SiW_9Co_3[h]$@ZIF-67

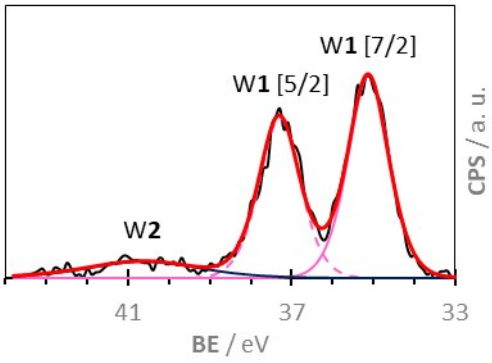

Figure S2. Deconvolutions of XPS high resolution C 1s, O 1s, Co 2p, Si 2s and W 4f core-level regions for the individual components (POMs and ZIF-67) and the four POM@ZIF-67 nanocomposites. Components are labelled as in Tables S1 and S2. Attributions, positions and FWHM for all the components are collected in Tables S1 and S2.

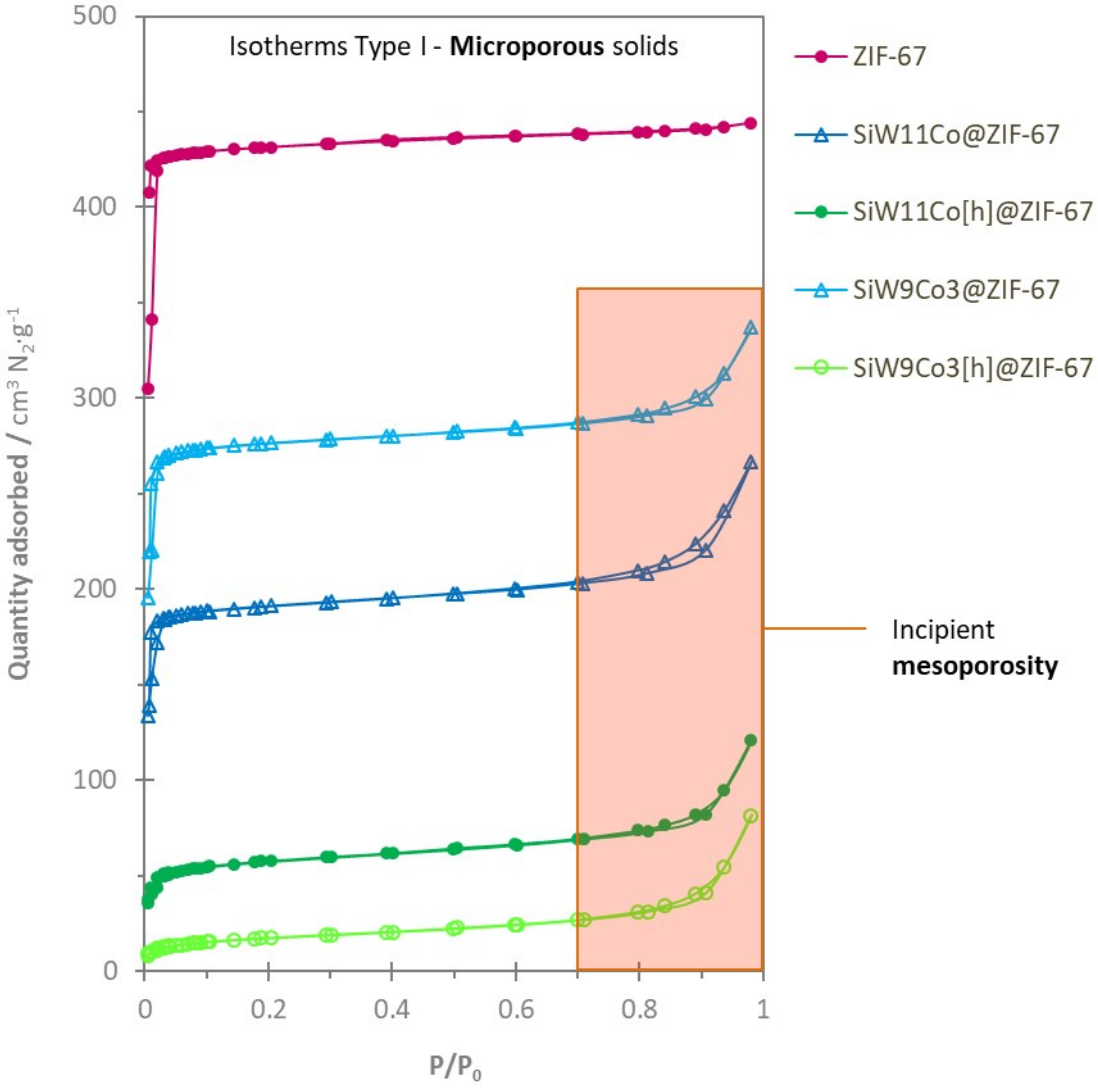

Figure S3. N_2-adsorption/desorption isotherm plots of ZIF-67 and POM@ZIF-67 nanocomposites.

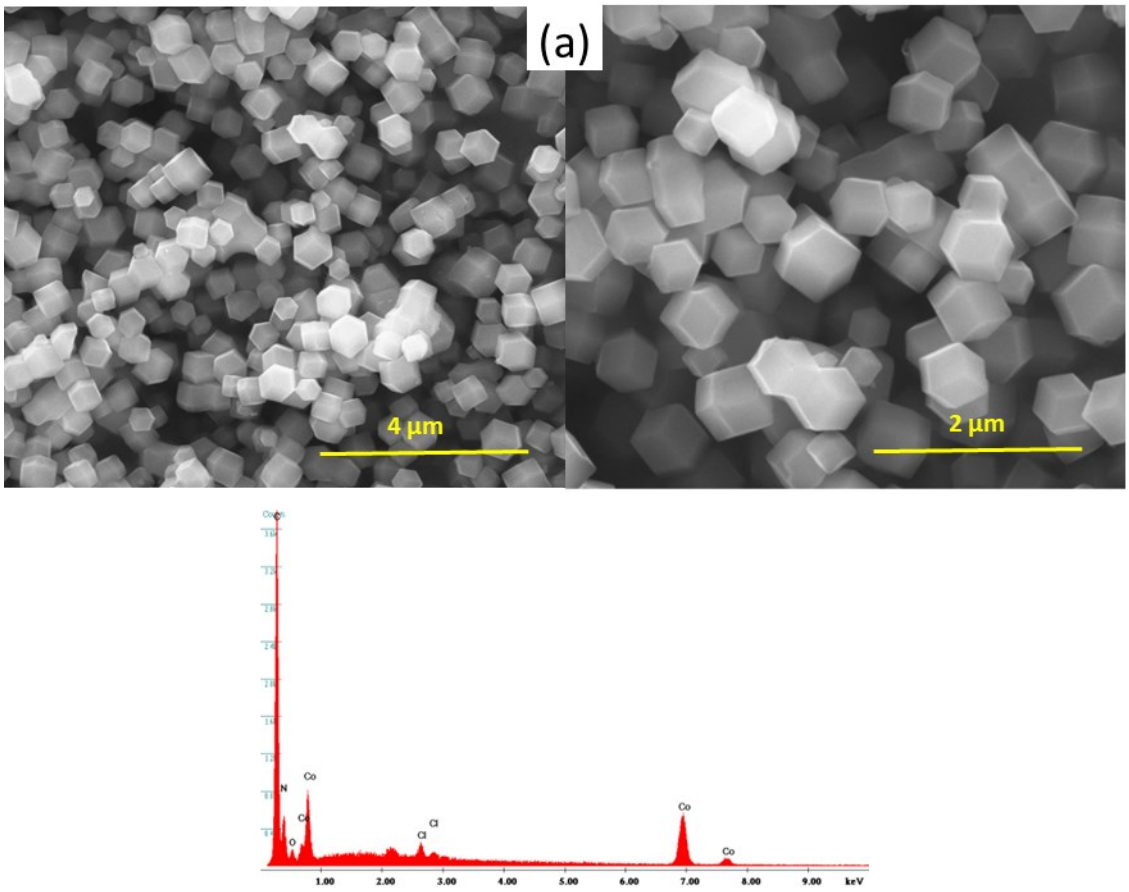
(a)
4 µm
2 µm
C
N
Co
O
Co
Cl
Cl
Co
Co
1.00
2.00
3.00
4.00
5.00
6.00
7.00
8.00
9.00
keV

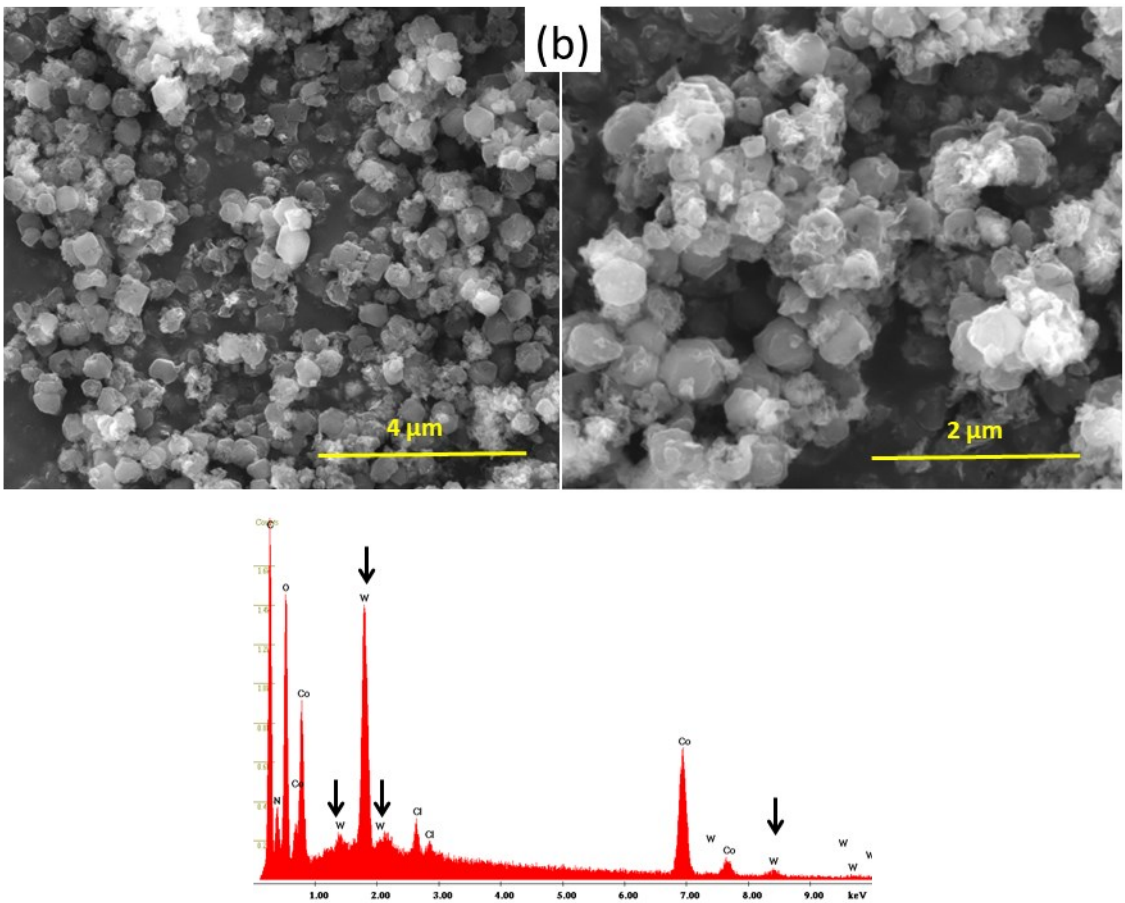
(b)
4 µm
2 µm
C
O
W
Co
N
Co
W
W
Cl
Cl
Co
W
Co
W
W
W
1.00
2.00
3.00
4.00
5.00
6.00
7.00
8.00
9.00
keV

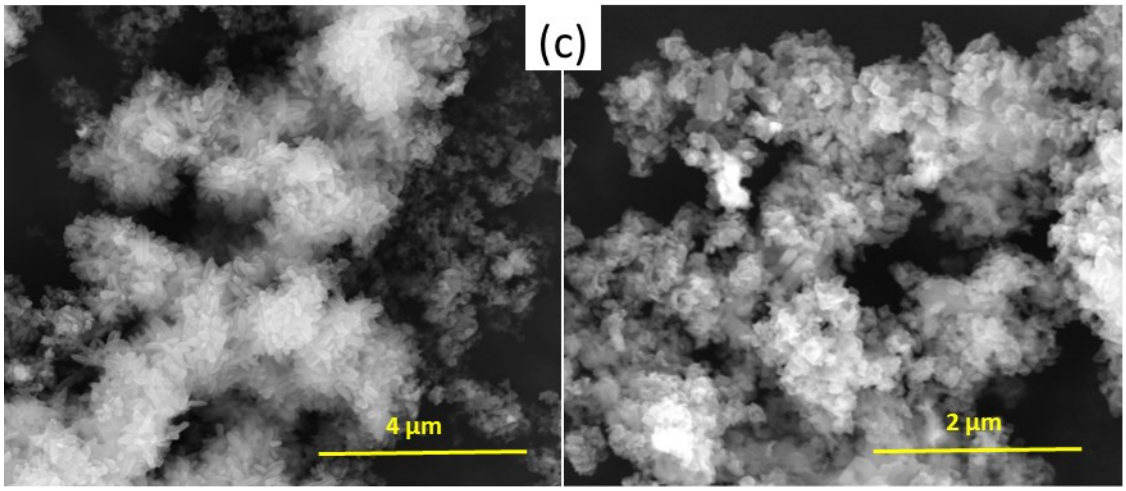
(c)
4 µm
2 µm

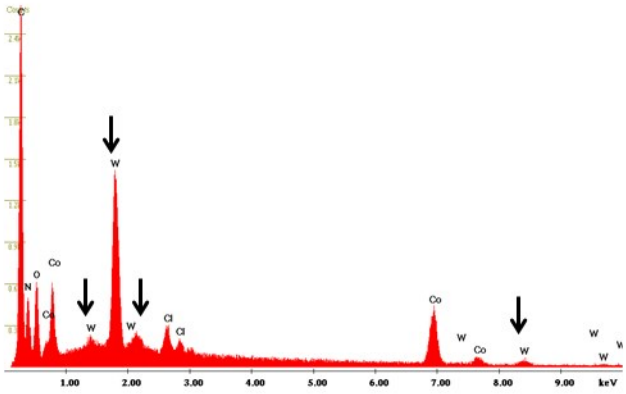
C
O
N
Co
W
Cl
1.00
2.00
3.00
4.00
5.00
6.00
7.00
8.00
9.00
keV

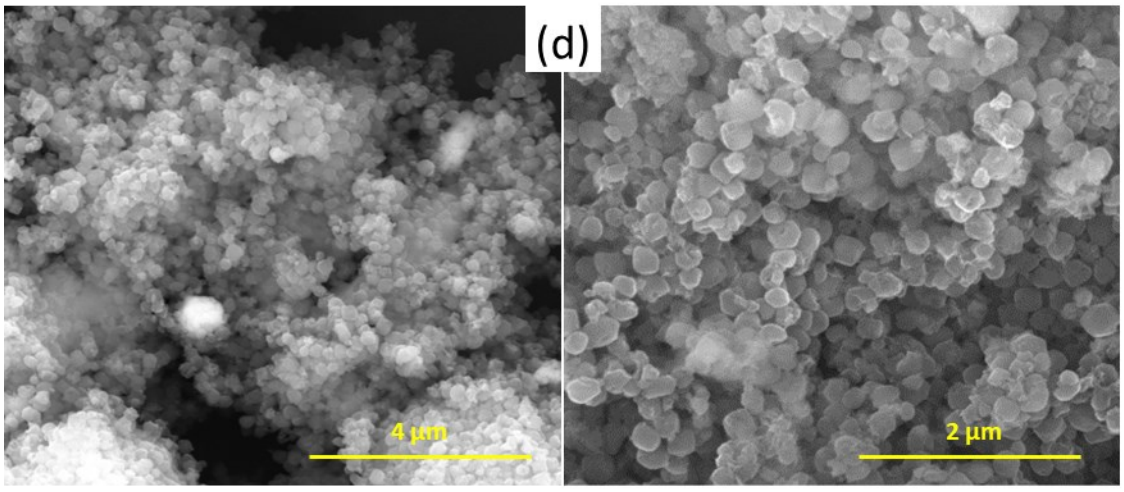
(d)
4 µm
2 µm

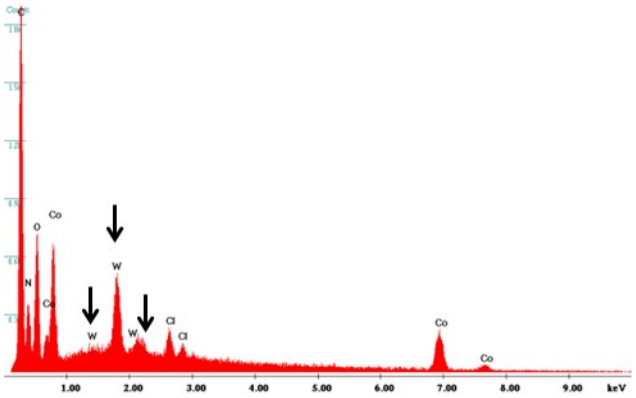
C
O
N
Co
W
Cl
1.00
2.00
3.00
4.00
5.00
6.00
7.00
8.00
9.00
keV

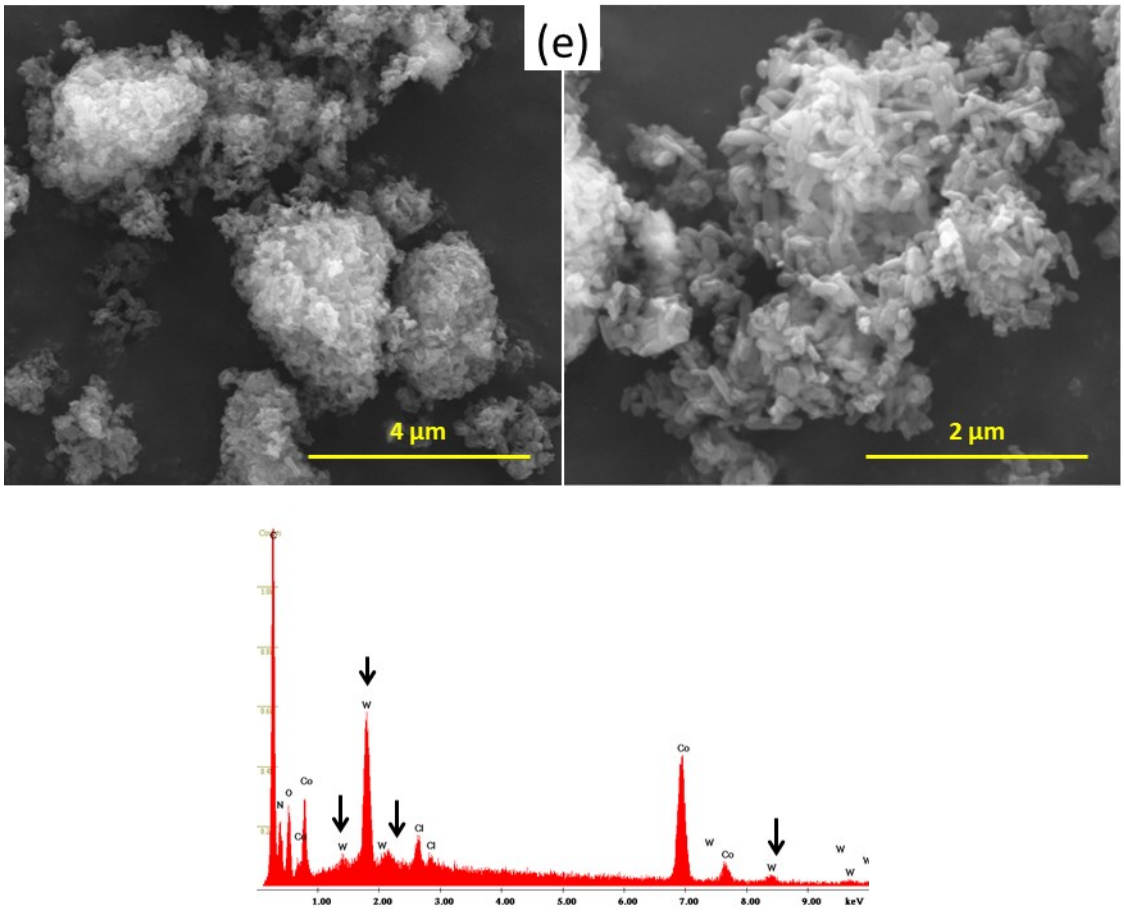

Figure S4. SEM micrographs and EDS spectra for **(a)** ZIF-67, **(b)** $SiW_{11}Co$@ZIF-67, **(c)** $SiW_{11}Co$[h]@ZIF-67, **(d)** SiW_9Co_3@ZIF-67, and **(e)** SiW_9Co_3[h]@ZIF-67. Si atoms from POM clusters are no detected due to their low concentration. *Black arrows point to W peaks (W atoms have POM clusters as unique origin).*

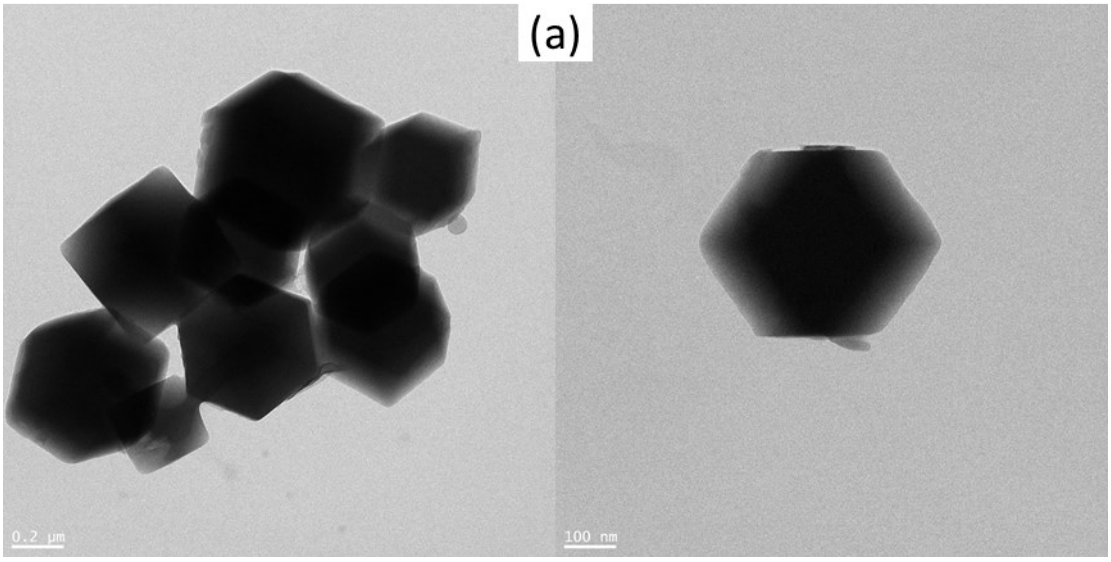

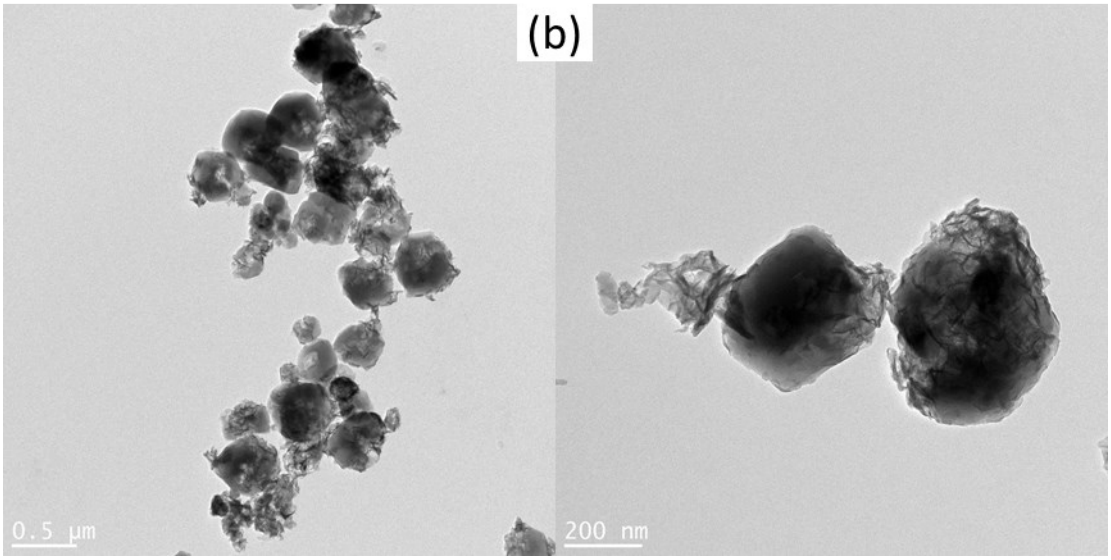
(b)
0.5 µm
200 nm

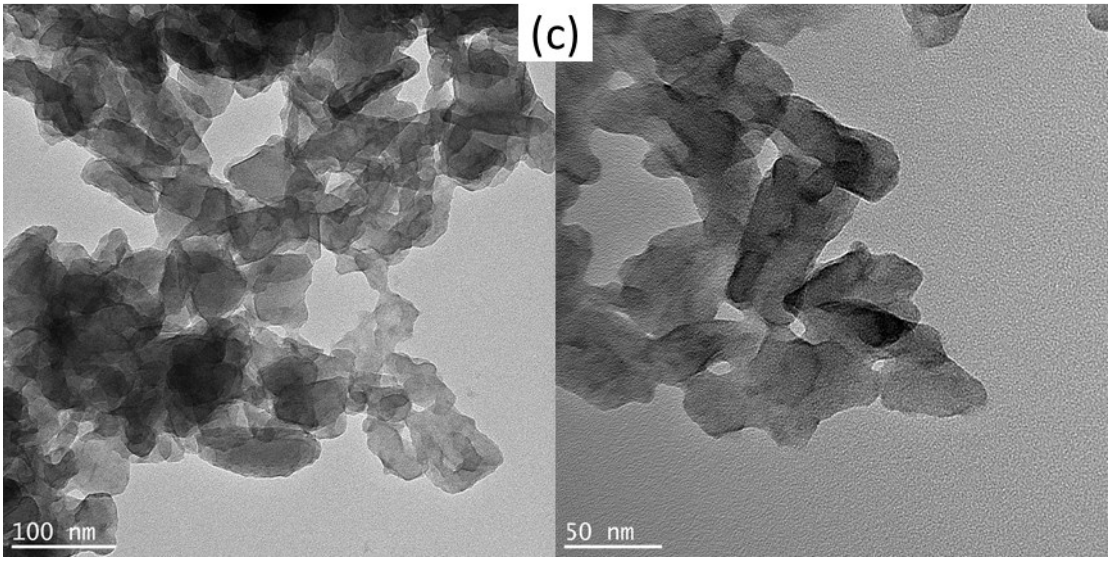
(c)
100 nm
50 nm

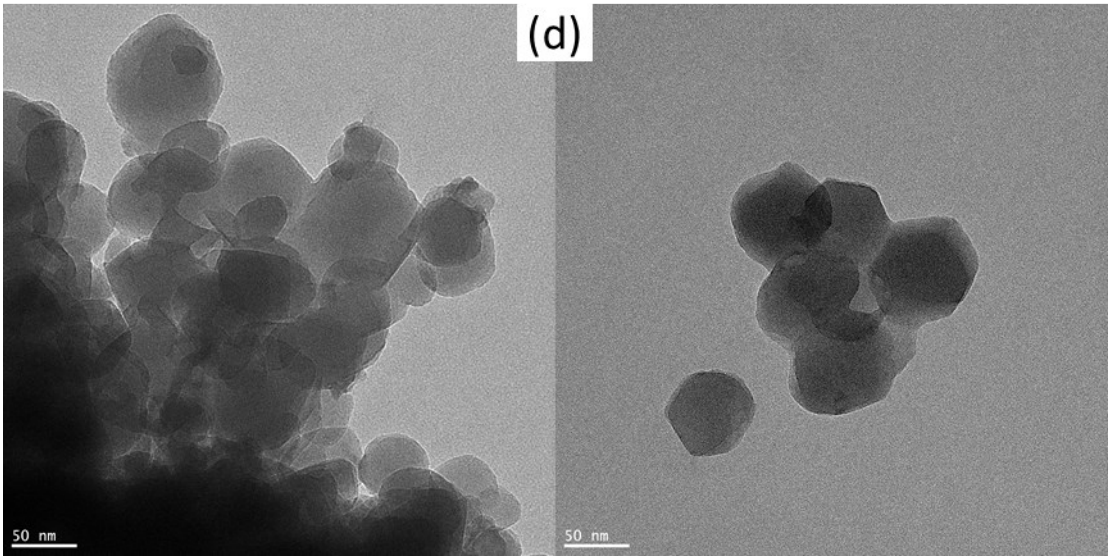
(d)
50 nm
50 nm

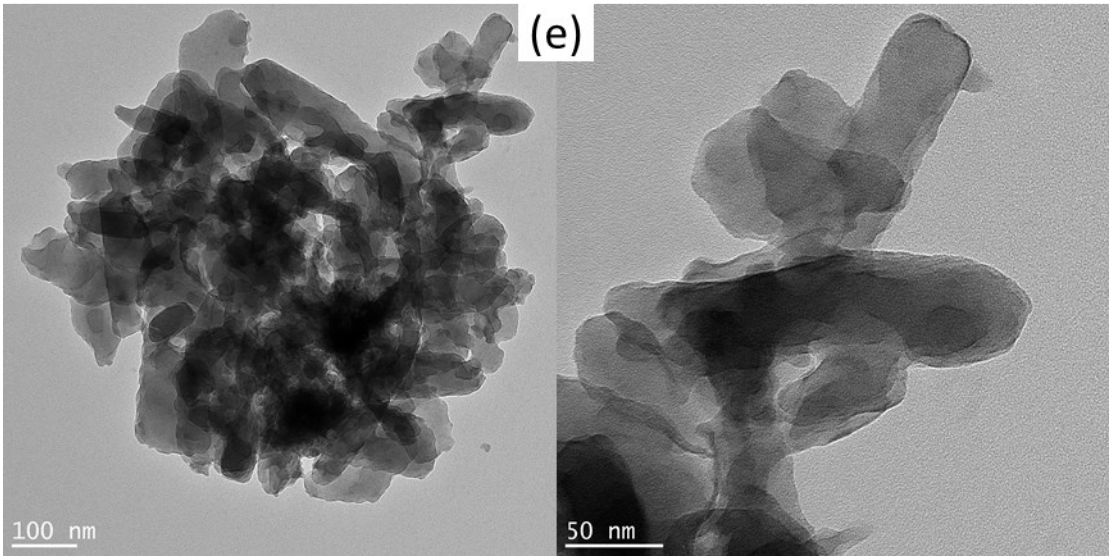

Figure S5. TEM images for **(a)** ZIF-67, **(b)** $SiW_{11}Co$@ZIF-67, **(c)** $SiW_{11}Co$[h]@ZIF-67, **(d)** SiW_9Co_3@ZIF-67, and **(e)** SiW_9Co_3[h]@ZIF-67.

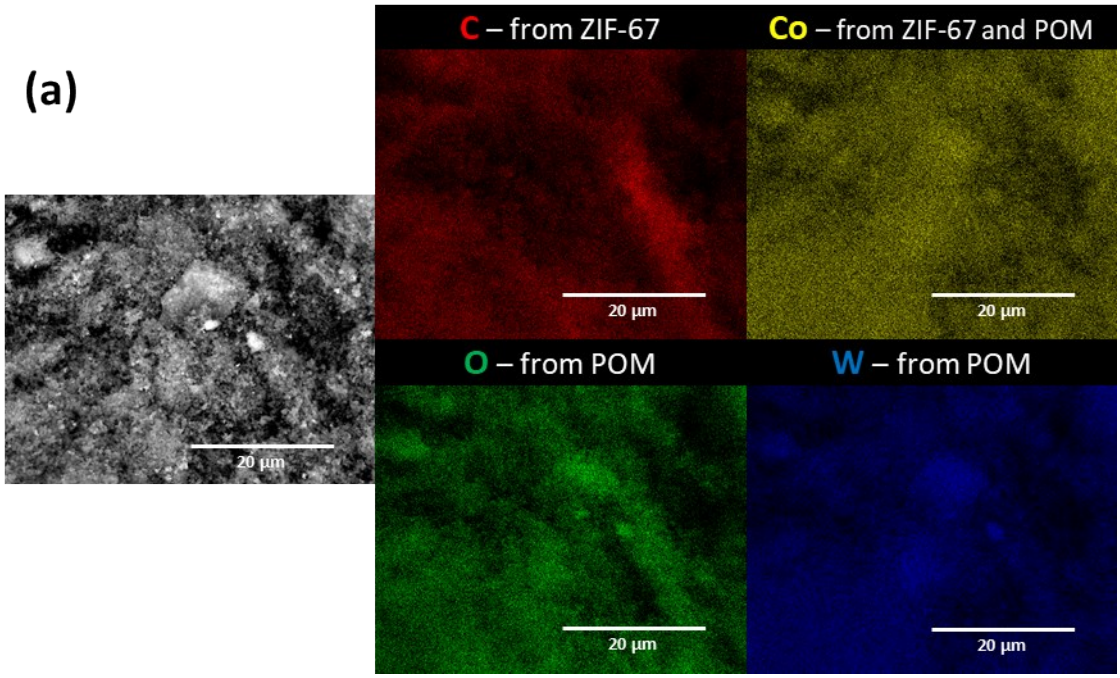

(b)

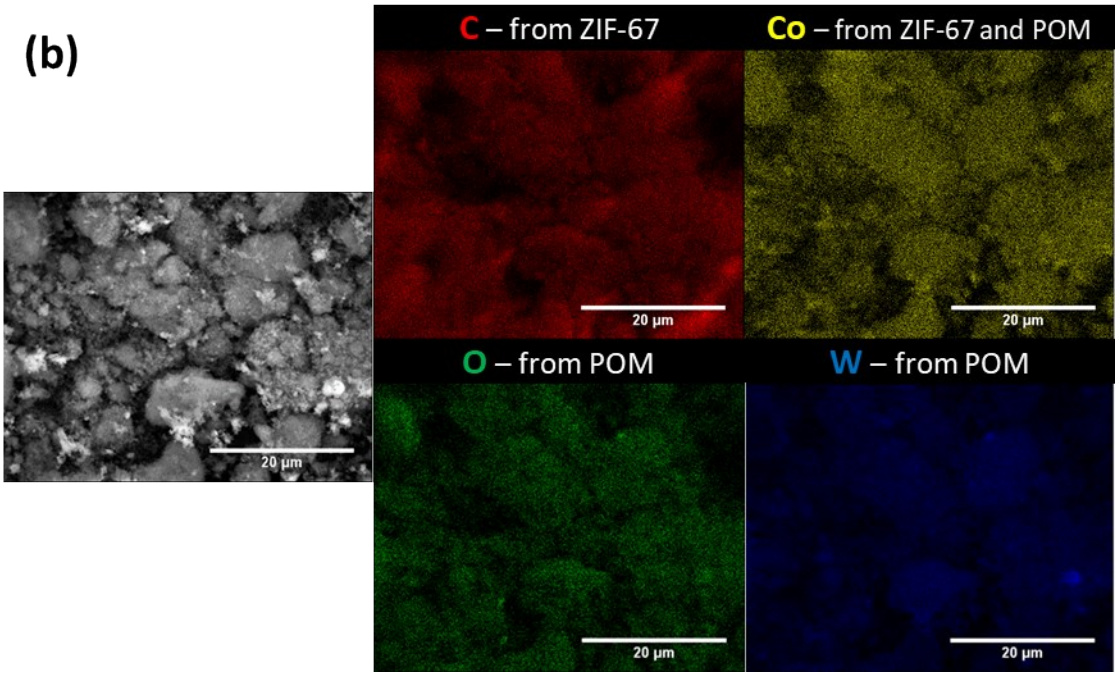
C – from ZIF-67
Co – from ZIF-67 and POM
O – from POM
W – from POM
20 µm

(c)

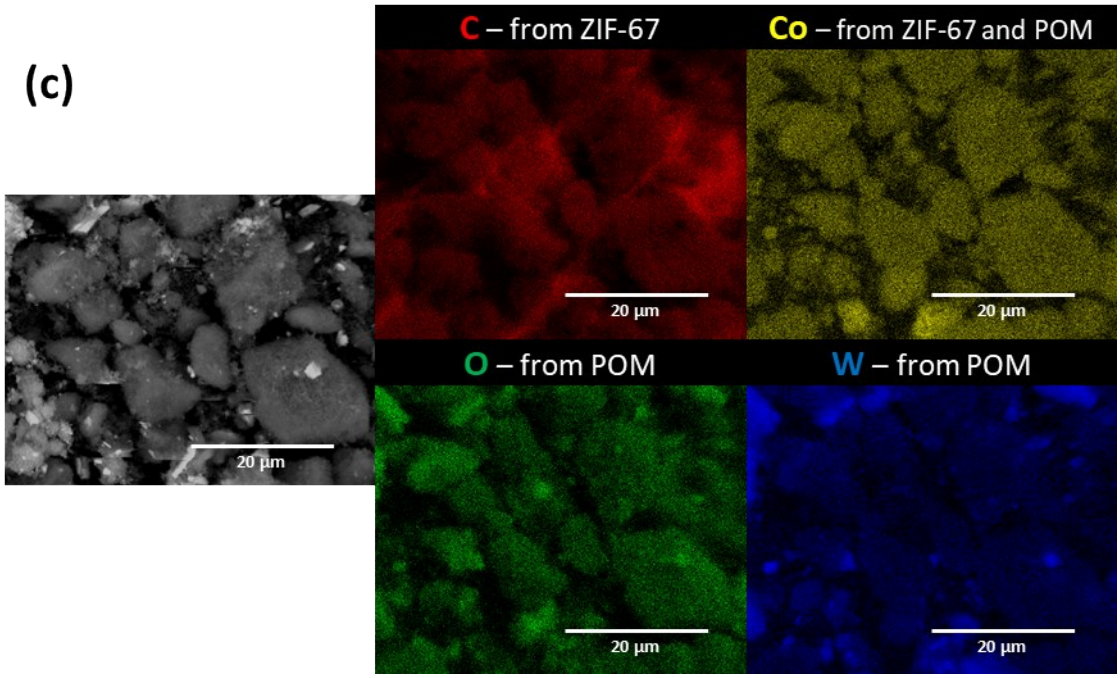
C – from ZIF-67
Co – from ZIF-67 and POM
O – from POM
W – from POM
20 µm

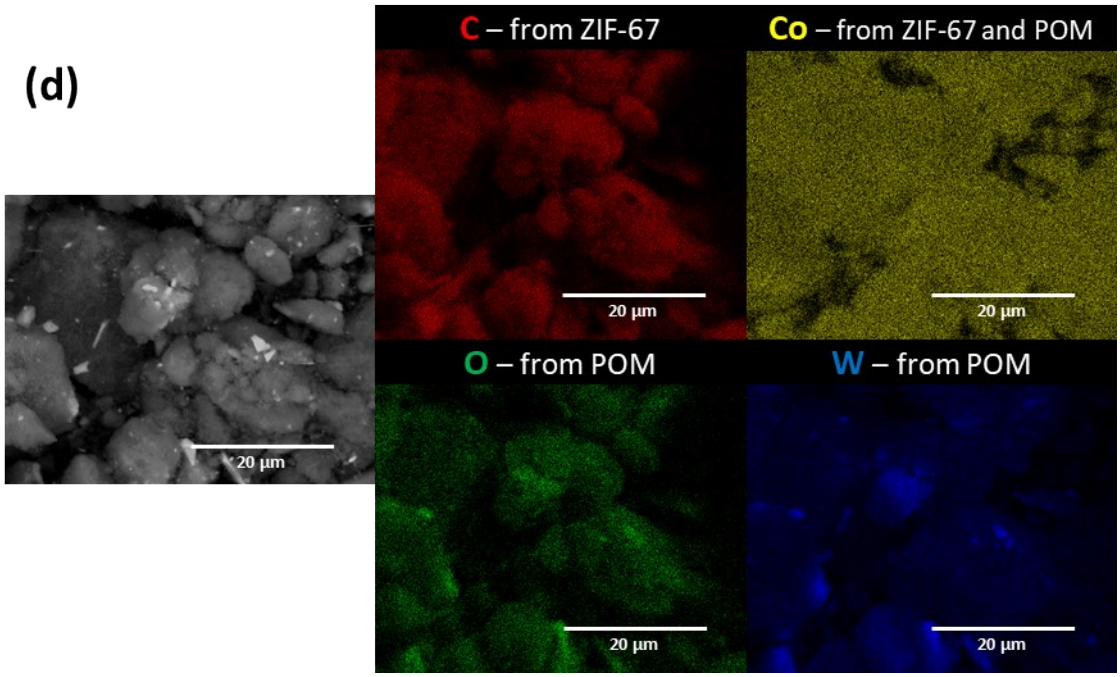

Figure S6. EDS-maps (SEM) of ZIF and POM elements for different nanocomposites: **(a)** $SiW_{11}Co$@ZIF-67, **(b)** $SiW_{11}Co$[h]@ZIF-67, **(c)** SiW_9Co_3@ZIF-67, and **(d)** SiW_9Co_3[h]@ZIF-67. Silicon from POM clusters is no detected due to its low concentration.

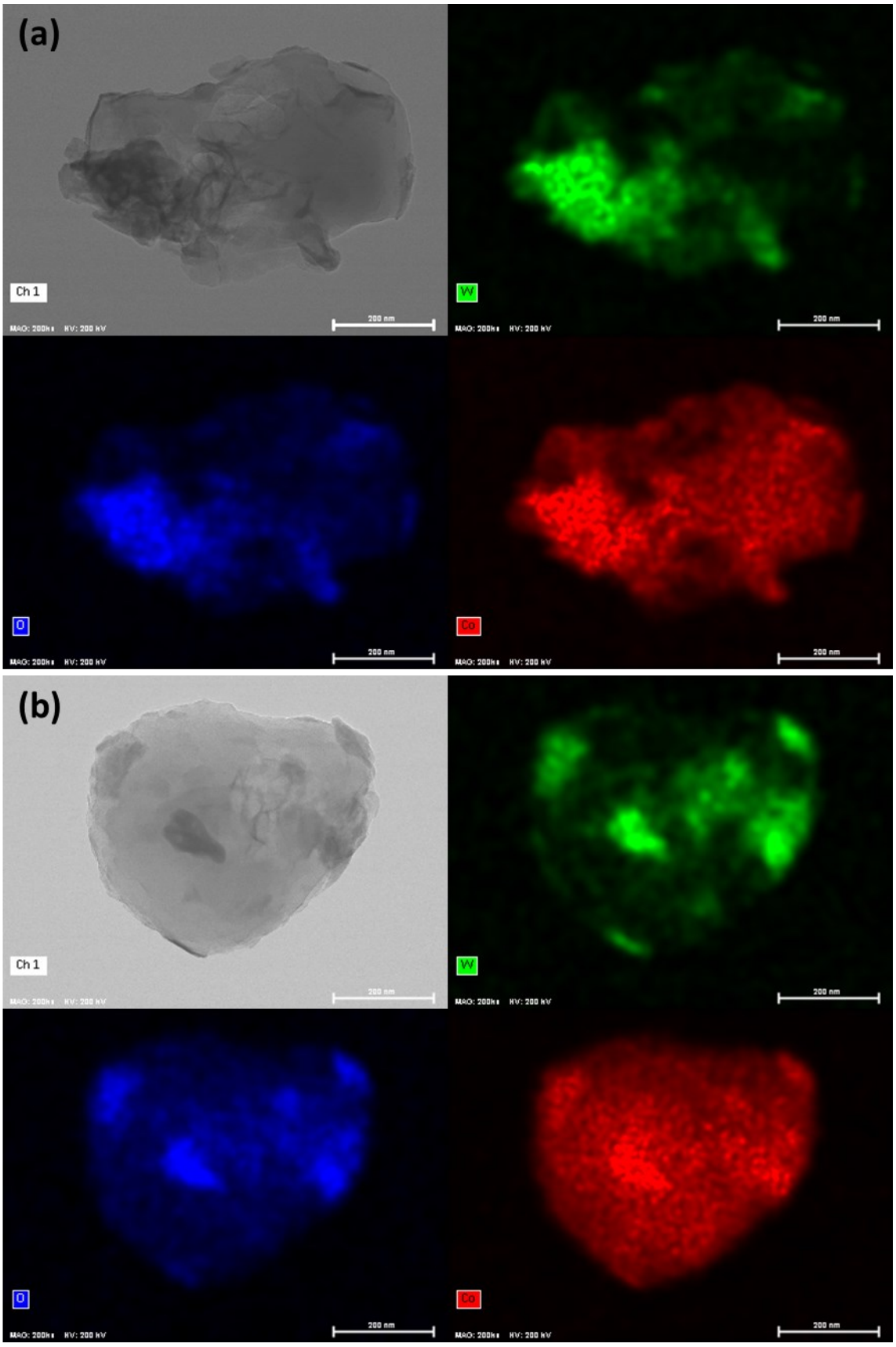
(a)
Ch 1
W
O
Co
(b)
Ch 1
W
O
Co

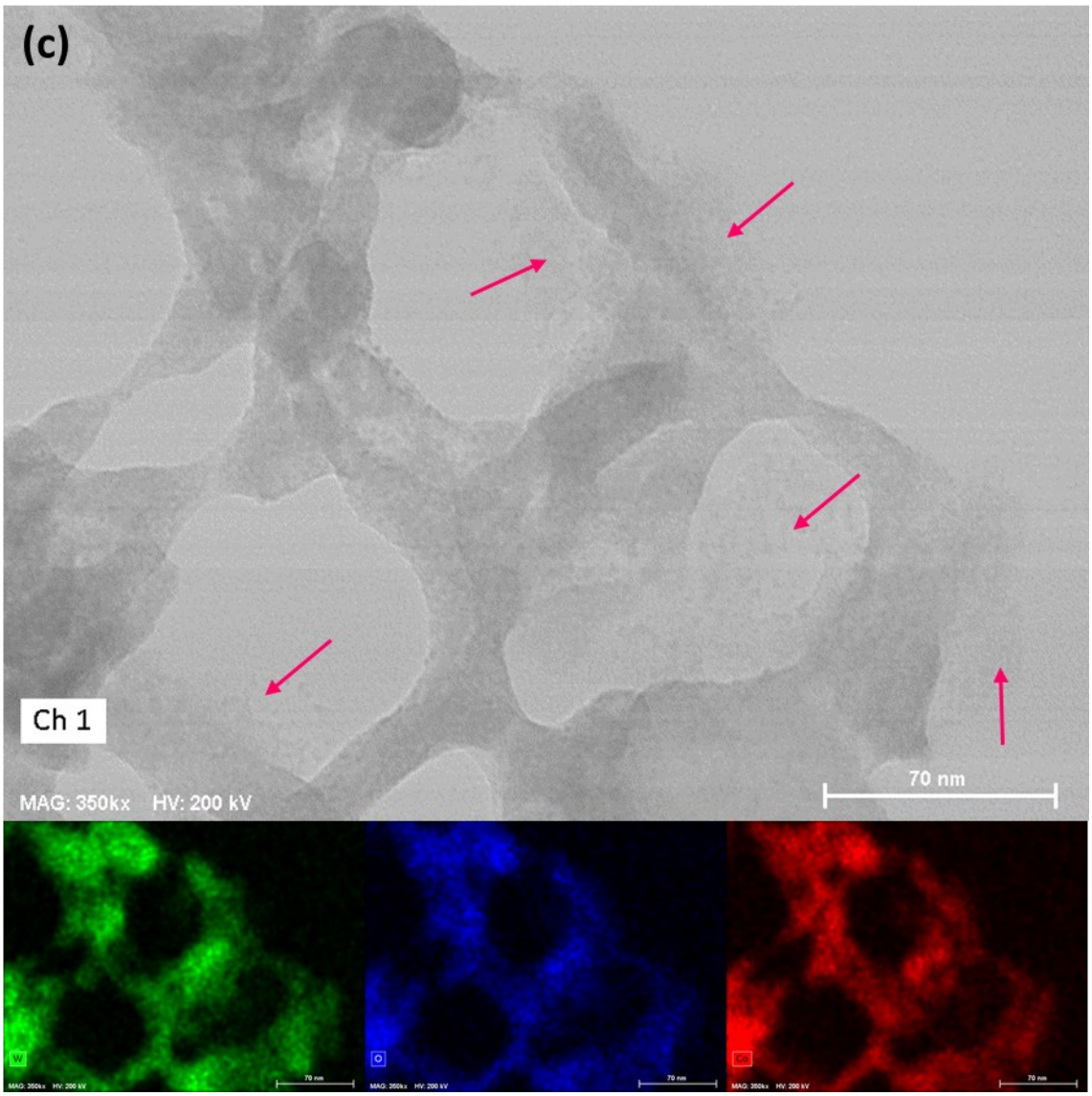

Arrows highlight the thin wrapping phase that surrounds the main structure.

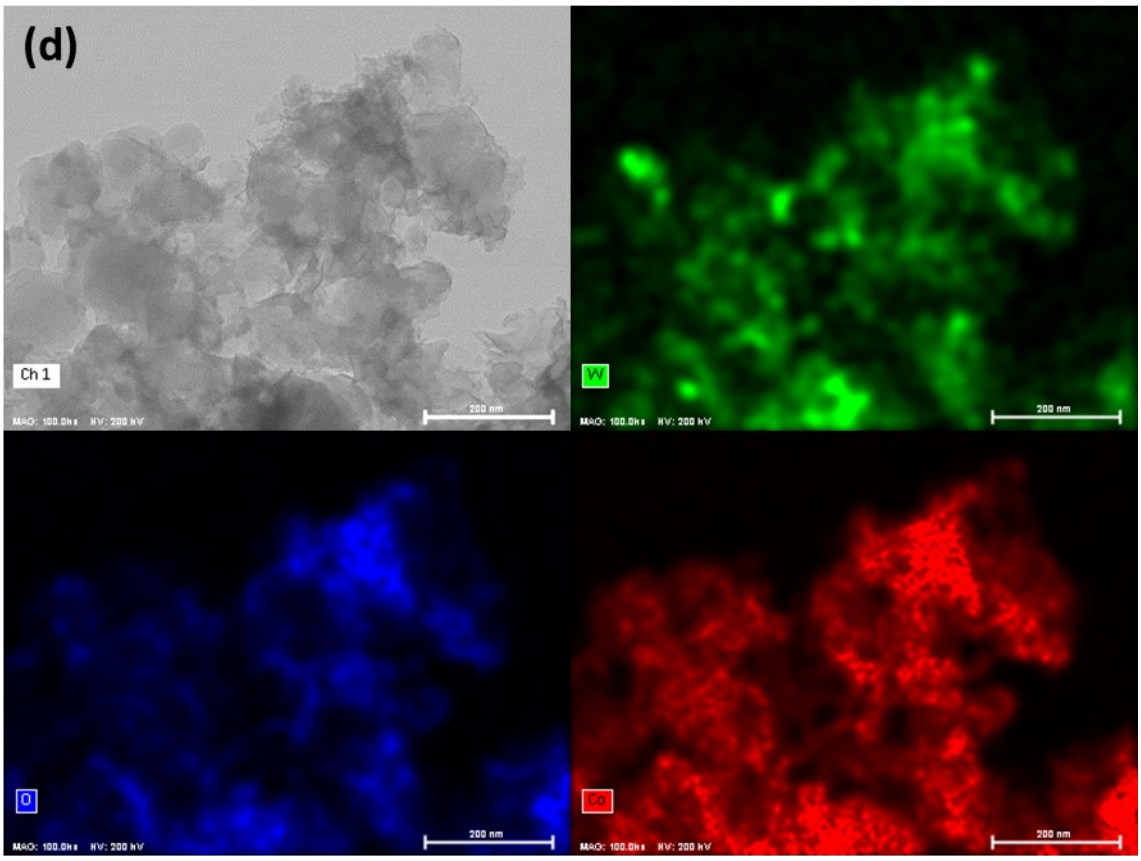
(d)
Ch 1
W
O
Co
200 nm

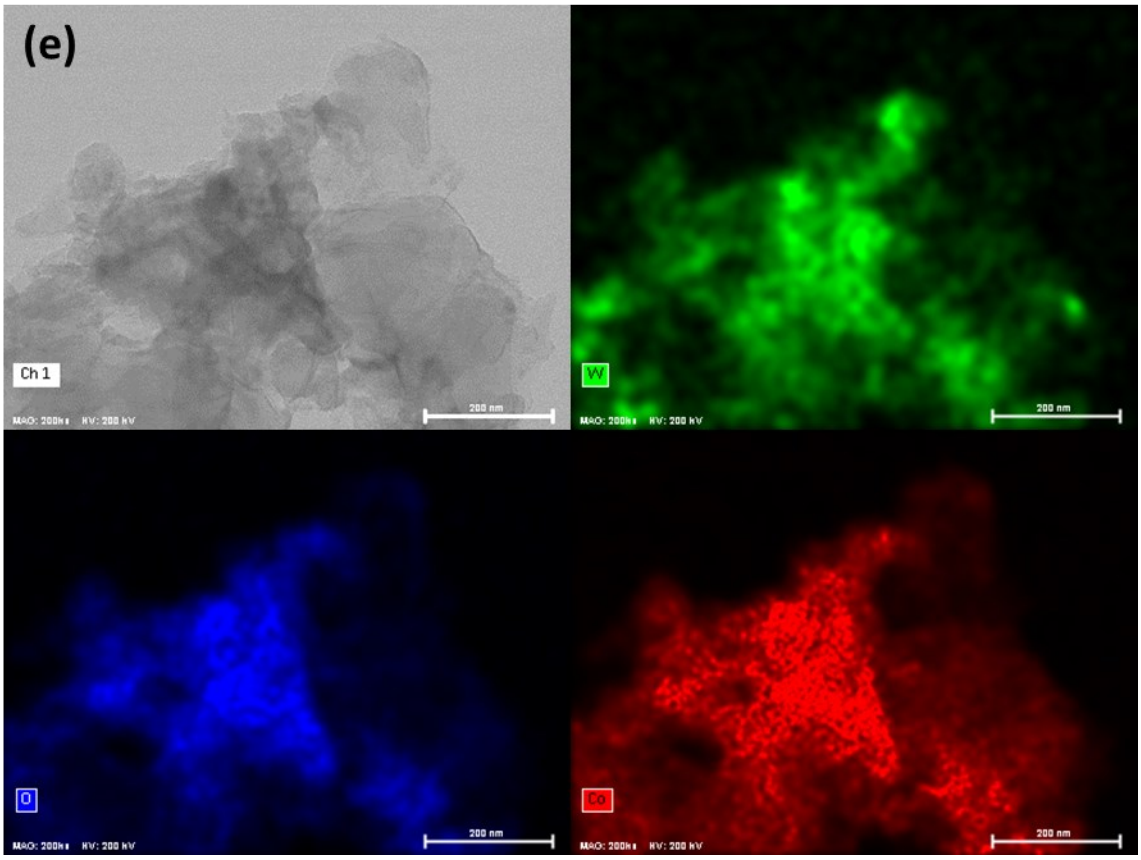
(e)
Ch 1
W
O
Co
200 nm

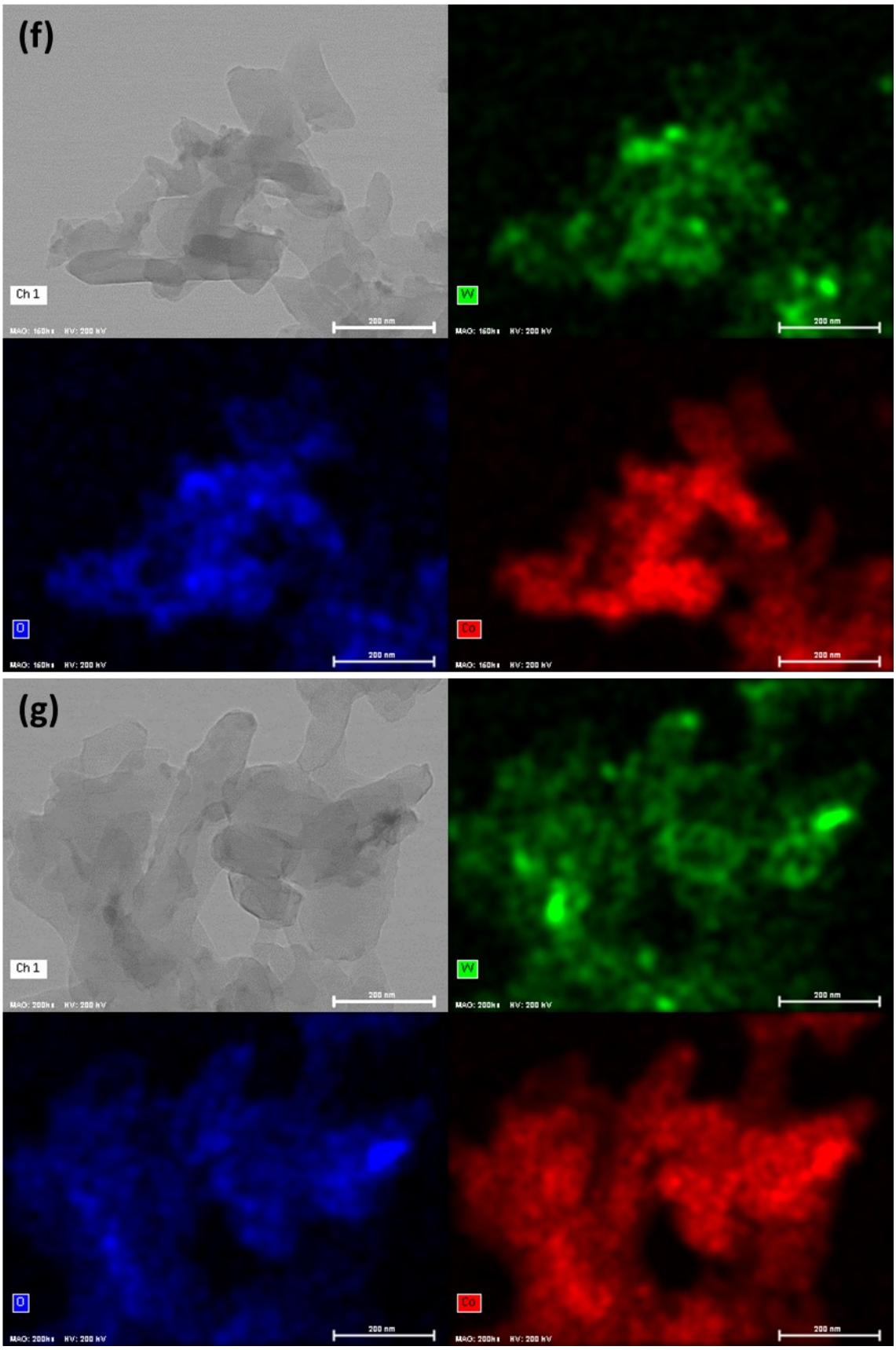
(f)
Ch 1
W
O
Co
(g)
Ch 1
W
O
Co

Figure S7. EDS element distribution maps (TEM) for the four nanocomposites: **(a,b)** $SiW_{11}Co$@ZIF-67, **(c)** $SiW_{11}Co$[h]@ZIF-67, **(d,e)** SiW_9Co_3@ZIF-67, and **(f,g)** SiW_9Co_3[h]@ZIF-67. **(c)** *Arrows highlight the thin wrapping phase that surrounds the main structure.* See other maps for $SiW_{11}Co$[h]@ZIF-67 in **Fig. 4** (in the article).

ZIF-67

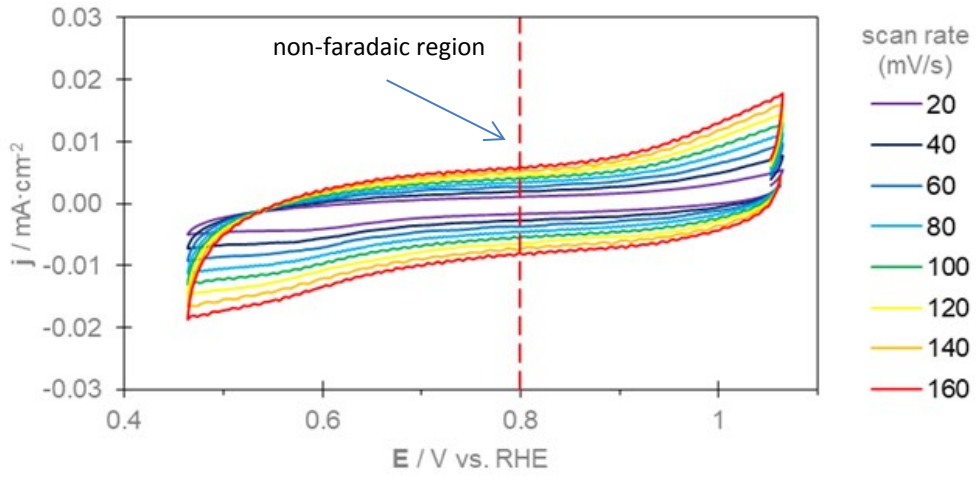

$SiW_{11}Co$@ZIF-67

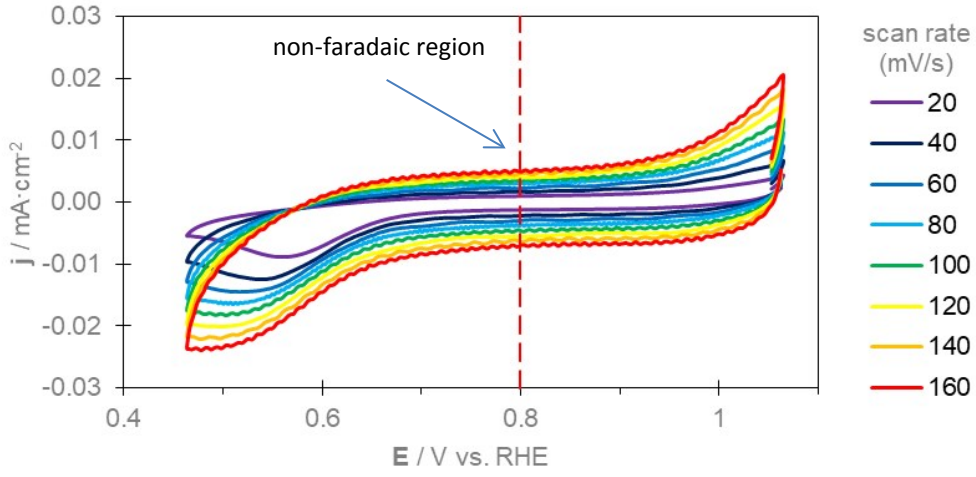

$SiW_{11}Co[h]@ZIF-67$

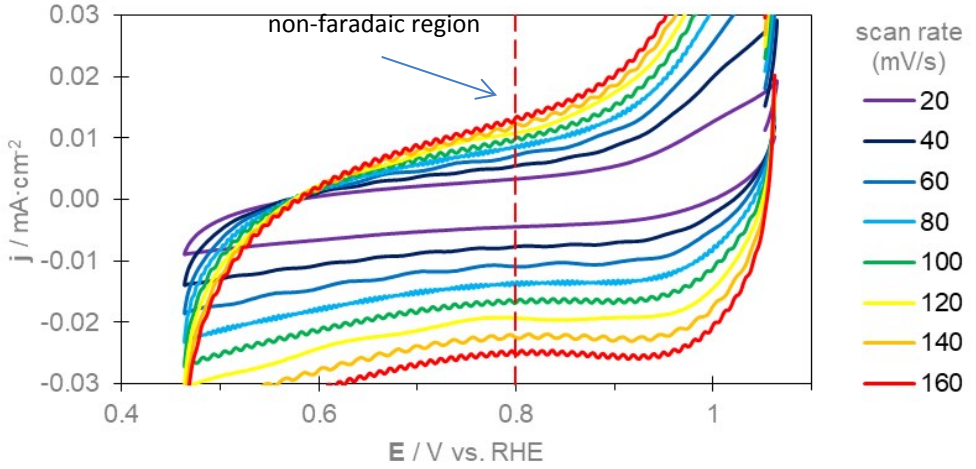

$SiW_9Co_3@ZIF-67$

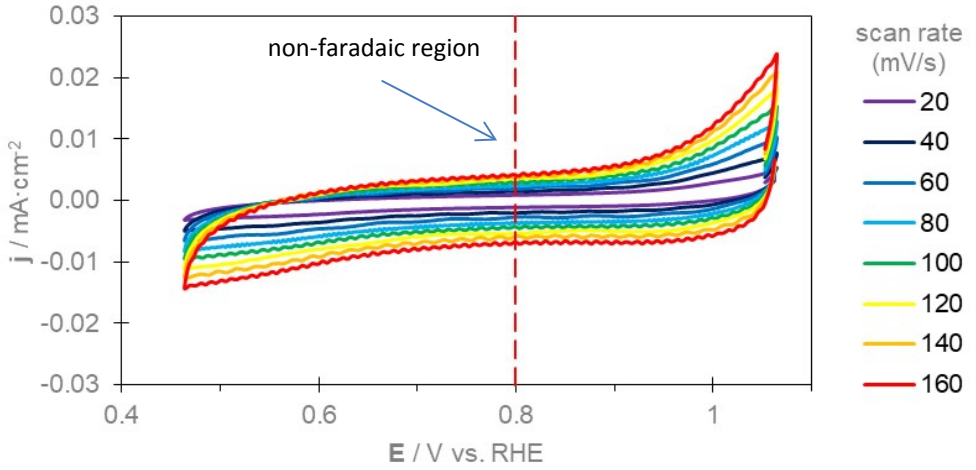

$SiW_9Co_3[h]@ZIF-67$

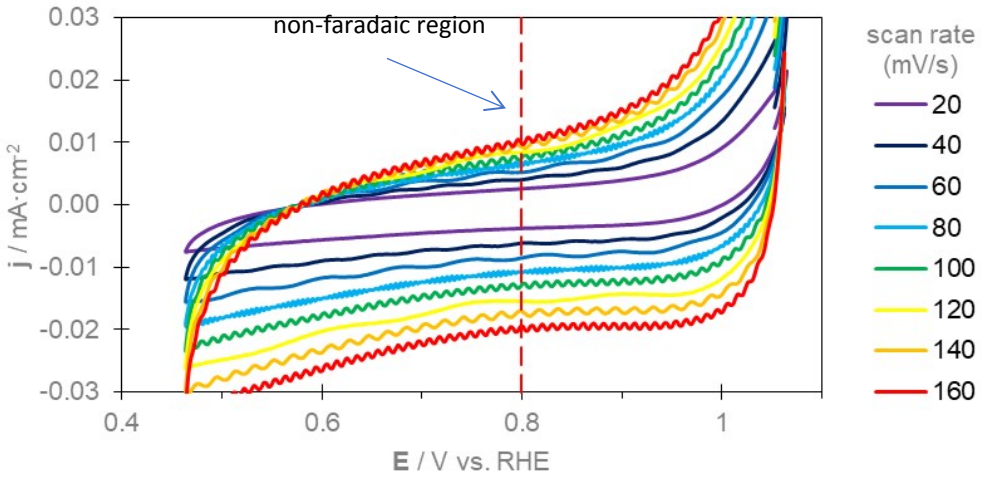

RuO_2

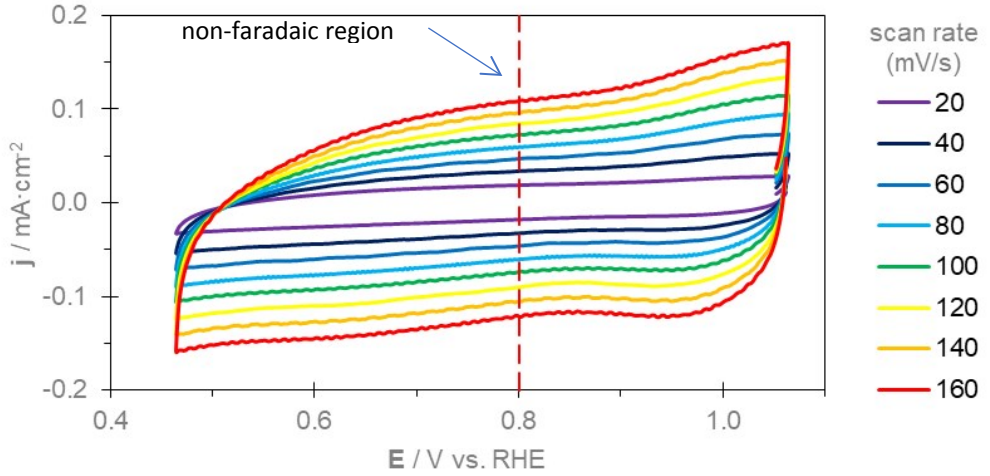

IrO_2

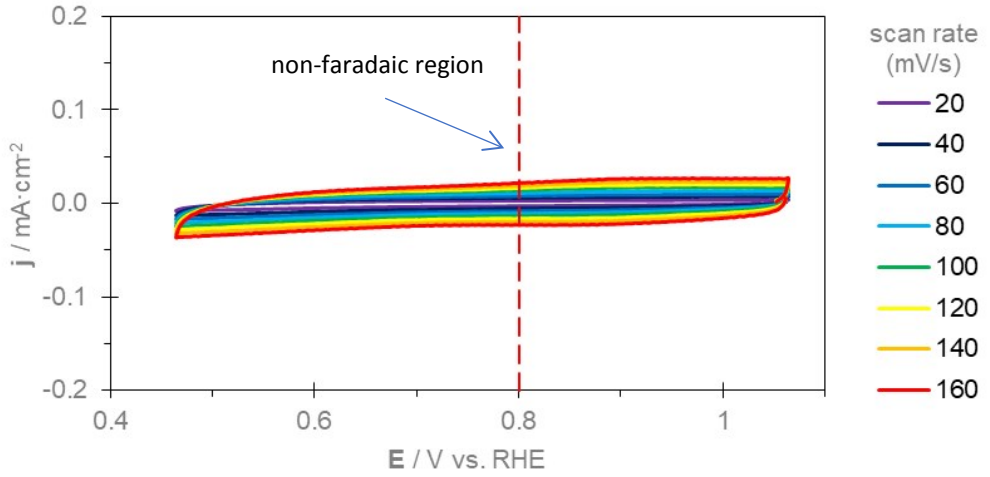

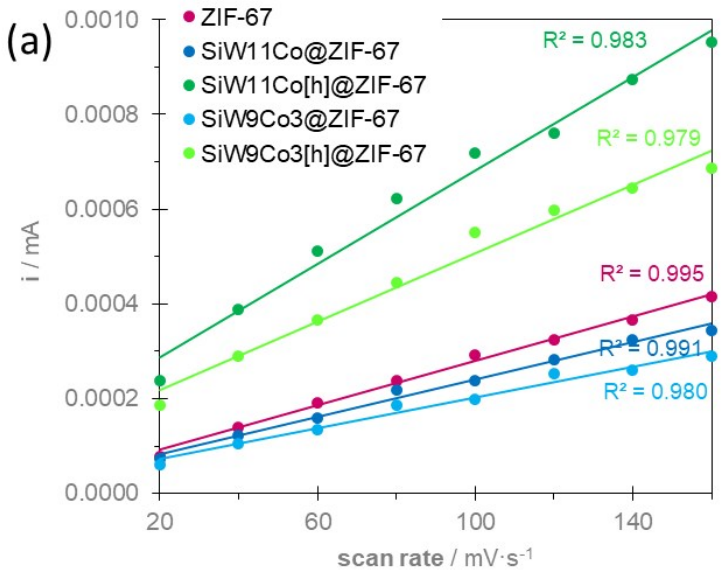

ZIF-67
$C_{dl} = 2.35 \cdot 10^{-6}$ F

$SiW_{11}Co$@ZIF-67
$C_{dl} = 1.97 \cdot 10^{-6}$ F

$SiW_{11}Co[h]$@ZIF-67
$C_{dl} = 4.93 \cdot 10^{-6}$ F

SiW_9Co_3@ZIF-67
$C_{dl} = 1.62 \cdot 10^{-6}$ F

$SiW_9Co_3[h]$@ZIF-67
$C_{dl} = 3.62 \cdot 10^{-6}$ F

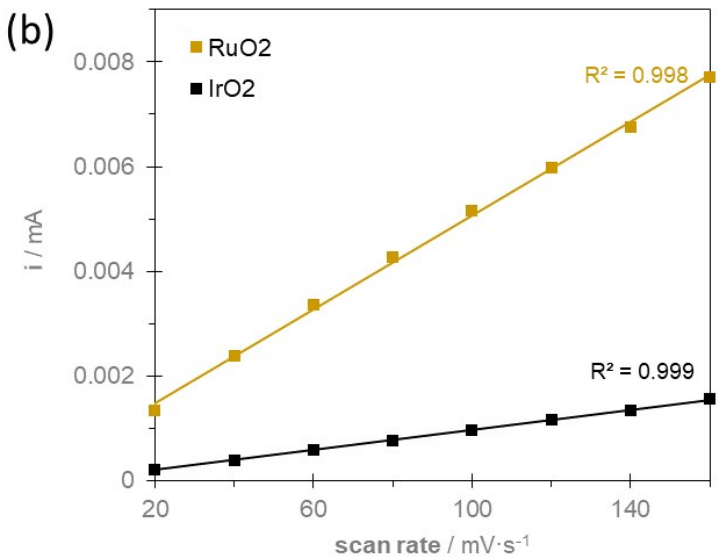

RuO_2
$C_{dl} = 4.47 \cdot 10^{-5}$ F

IrO_2
$C_{dl} = 9.60 \cdot 10^{-6}$ F

Figure S8. CV plots at different scan rates (N_2-saturated KOH 0.1 M electrolyte) for the pristine ZIF-67, POM@ZIF-67 nanocomposites, and benchmark materials. And their corresponding linear fitting plots **(a** and **b)** with slope values, C_{dl}.

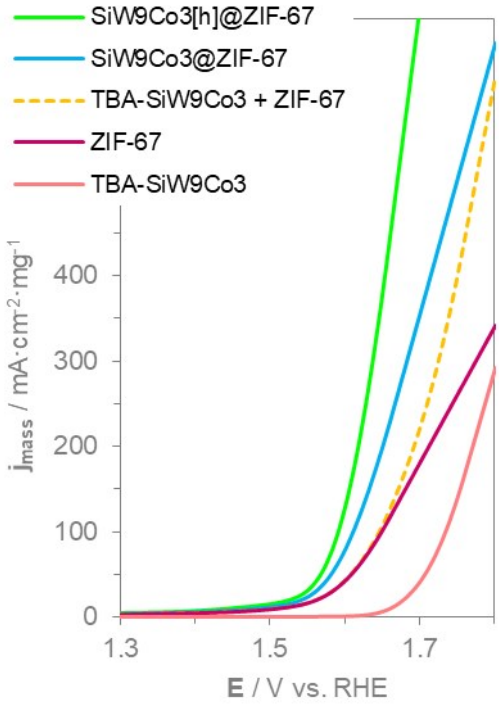

Figure S9. Mass-normalized LSV polarization curves for the OER electrocatalysis of SiW_9Co_3-containing materials. The dashed line represents the sum of the 'individual' components, TBA-SiW_9Co_3 and ZIF-67.

REFERENCES

1. V. K. Abdelkader Fernández, D. Mesquita Fernandes, S. Silva Balula, L. Cunha-Silva and C. Freire, *ACS Applied Energy Materials*, 2020, **3**, 2925-2934.
2. S. S. Balula, L. Cunha-Silva, I. Santos, A. C. Estrada, A. C. Fernandes, J. A. S. Cavaleiro, J. Pires, C. Freire and A. M. V. Cavaleiro, *New Journal of Chemistry*, 2013, **37**, 2341-2350.
3. S. Jung, C. C. L. McCrory, I. M. Ferrer, J. C. Peters and T. F. Jaramillo, *Journal of Materials Chemistry A*, 2016, **4**, 3068-3076.
4. T. F. S. Inc., XPSsimplified, https://xpssimplified.com/).
5. A. Awadallah-F, F. Hillman, S. A. Al-Muhtaseb and H. K. Jeong, *Journal of Materials Science*, 2019, **54**, 5513-5527.
6. F. Y. Tian, A. M. Cerro, A. M. Mosier, H. K. Wayment-Steele, R. S. Shine, A. Park, E. R. Webster, L. E. Johnson, M. S. Johal and L. Benz, *Journal of Physical Chemistry C*, 2014, **118**, 14449-14456.
7. Q. P. Dai, J. F. Zhang and M. Ma, *Applied Surface Science*, 1993, **72**, 67-72.
8. S. Aduru, S. Contarini and J. W. Rabalais, *Journal of Physical Chemistry*, 1986, **90**, 1683-1688.
9. K. Burger, F. Tschimarov and H. Ebel, *Journal of Electron Spectroscopy and Related Phenomena*, 1977, **10**, 461-465.
10. D. N. Hendrickson, J. M. Hollander and W. L. Jolly, *Inorganic Chemistry*, 1969, **8**, 2642-+.
11. L. L. Xiao, Q. Zhao, L. Jia, Q. Chen, J. Jiang and Q. Y. Yu, *Electrochimica Acta*, 2019, **304**, 456-464.
12. N. Joo, Université Joseph-Fourier, 2011.